

AD 642155

NPL AERO REPORT 1189

UNLIMITED

NPL AERO REPORT 1189

A. R. C. 27 832

A. R. C. 27 832

F. M. 3693

F. M. 3693

Perf. 2475

Perf. 2475

P. A. 1155

P. A. 1155

## NATIONAL PHYSICAL LABORATORY

### AERODYNAMICS DIVISION

THE FLOW ABOUT A FAMILY OF SIMPLE, BLUNT  
AND SHARP LEADING-EDGED, TWO-DIMENSIONAL  
AEROFOILS AT TRANSONIC AND LOW SUPERSONIC SPEEDS

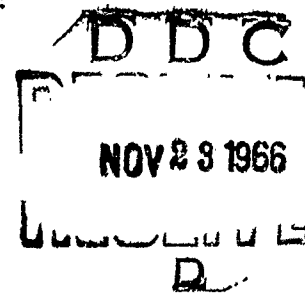
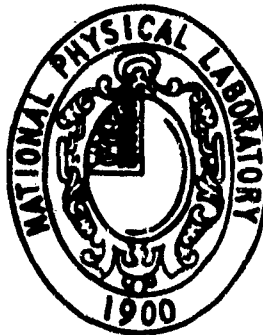
by

W. J. Graham

28th February, 1966

THE RECIPIENT IS WARNED THAT INFORMATION  
CONTAINED IN THIS DOCUMENT MAY BE SUBJECT  
TO PRIVATELY-OWNED RIGHTS.

CLEARINGHOUSE FOR FEDERAL SCIENTIFIC AND TECHNICAL INFORMATION			
Hardcopy	Microfiche		
3.00	1.65	59	20
/ ARCHIVE COPY			



A Station of the  
Ministry of Technology

Crown Copyright Reserved

ACCESSION TO	
QSTI	WHITE SECTION <input checked="" type="checkbox"/>
BDC	BUFF SECTION <input type="checkbox"/>
UNANNOUNCED	<input type="checkbox"/>
JUSTIFICATION	
BY	
DISTRIBUTION/AVAILABILITY CODES	
DIST.	AVAIL. and/or SPECIAL
/	

The work described in this paper forms part of the research programme carried out by the Aerodynamics Division of the National Physical Laboratory for the Ministry of Aviation

Approved on behalf of Director, NPL by  
Dr. R. C. Pankhurst, Superintendent of Aerodynamics Division

A.R.C. 27 838

AERONAUTICAL RESEARCH COUNCIL

A.R.C. 27 838

F.M. 3693  
Perf. 2475  
P.A. 1155

FLUID MOTION SUB-COMMITTEE

F.M. 3693  
Perf. 2475  
P.A. 1155

The Flow about a Family of Simple, Blunt and Sharp  
Leading-Edged, Two-Dimensional Aerofoils at  
Transonic and Low Supersonic Speeds

- By -

W. J. Graham

---

28th February, 1966

SUMMARY

The flow about the aerofoils is examined with particular attention to the expansive flow, to supersonic speeds, on the blunt leading edges, and to the subsequent compression. The movements of stagnation and sonic points are analysed. The shock structure in the supersonic compression process is explained, with the aid of a characteristics network. The effects of blunting on lift and lift-drag ratio are considered.

---

List/

List of Contents

	<u>Page</u>
Notation .. .. .	..
1. Introduction .. .. .	1
2. Wind Tunnel and Models .. .. .	6
3. Test Conditions .. .. .	8
4. Inviscid Flow Behind a Blunt Leading Edge .. .. .	10
5. Discussion of the Flow about the Aerofoils .. .. .	11
6. Pressure Distributions .. .. .	12
6.1 Results on the sharp aerofoil at $M_0 = 1$ , $\alpha = 0$ .. .. .	12
6.2 Results on the sharp and blunt aerofoils .. .. .	13
6.3 Effects of fixing boundary-layer transition .. .. .	14
7. Induced Pressure Differences due to Leading-Edge Blunting .. .. .	15
8. Flow about the Leading-Edge Cylinders .. .. .	16
8.1 Pressure distributions .. .. .	16
8.2 Comparison with theory .. .. .	17
8.3 Movement of stagnation point .. .. .	18
8.4 Movement of sonic point .. .. .	19
9. Lift Coefficients and Lift-Drag Ratios .. .. .	20
10. Effects of Tunnel-Wall Interference .. .. .	21
11. Conclusions .. .. .	22
Acknowledgements .. .. .	23
References .. .. .	24

Notation

M	Mach number
p	static pressure
H	total pressure
c	aerofoil chord (general)
a	chord of sharp leading-edged aerofoil (R30)
r	leading-edge radius

- x chordwise co-ordinate measured from leading edge
- $\zeta$  chordwise co-ordinate measured from the discontinuity of curvature
- z thickness co-ordinate measured from the axis of symmetry
- $\alpha$  angle of incidence
- r thickness-chord ratio
- $\theta$  surface slope
- $\bar{\theta}$  angular co-ordinate measured from the axis of symmetry,  
=  $90 - \theta$

$$C_p \quad \text{pressure coefficient} = \frac{p - p_o}{\frac{1}{2} \gamma p_o M_o^2}$$

$$\bar{C}_p \quad \text{reduced pressure coefficient} = C_p \frac{[M_o^2 (\gamma + 1)]^{1/3}}{\gamma^2 s}$$

$$\xi_o \quad \text{transonic similarity parameter,} = \frac{1 - M_o^2}{[(\gamma + 1) \gamma M_o^2]^{2/3}}$$

$\gamma$  ratio of specific heats

k rate of angular movement of stagnation point with incidence

$$C_L \quad \text{lift coefficient,} = \frac{\text{Lift}}{\frac{1}{2} \gamma p_o M_o^2}$$

$$C_D \quad \text{drag coefficient,} = \frac{\text{Pressure Drag}}{\frac{1}{2} \gamma p_o M_o^2}$$

$\sigma$  liner open-area ratio

h tunnel height

$$2\ell \quad \text{slot spacing,} = \frac{\text{Tunnel Width}}{\text{Number of slots}}$$

$$C = - \frac{2\ell}{\pi} \ln \sin \frac{\pi \sigma}{2}$$

$$T \quad \text{tunnel liner parameter,} = \frac{1 - (C/h)}{1 + (C/h)}$$

Subscripts/

### Subscripts

- o free-stream value
- s stagnation point value

### Subscript

- \* sonic point value

## 1. Introduction

The work described in this paper is aimed at the development of aerofoil sections which, at transonic speeds, have extensive regions of local supersonic flow but have only weak shock waves and so maintain satisfactory performance characteristics. It is thus hoped to relax the severe restrictions on thickness-chord ratio and minimum sweep-angle which apply when the onset of strong shock waves is avoided by preventing extensive regions of local supersonic flow.

Pressure distributions, on a wide range of aerofoil shapes which give rise to local regions of supersonic flow, fall into the two main categories sketched in Fig. 1: (a) those for which there is a monotonic reduction in pressure from the stagnation point, through sonic pressure, to a shock wave and (b) those for which there is a rapid reduction in pressure to supersonic values near the leading edge, followed by a general rise in pressure towards the shock wave. The latter type of pressure distributions have become known as "peaky" since they are associated with high velocity peaks. The shock wave referred to here is, in general, required to match the local supersonic flow to the subsonic downstream flow. The type of pressure distribution achieved is found to depend on the section geometry, the angle of incidence and the free-stream Mach number. The possibilities of utilising the pressure distributions of the second type to bring about significant improvements in transonic aerofoil performance, through improved lift, drag-rise Mach number and separation characteristics, have been shown by Pearcey<sup>1</sup> and in recent years much effort has been devoted to the understanding of the flow mechanism and controlling factors.

One obvious role of the low pressure region on the upper surface is to increase the lift, by an amount proportional to the difference between the areas within the upper- and lower-surface pressure distributions (Fig. 1). In addition the low pressures in the "peak" region act, at least in part, to reduce the pressure drag<sup>1</sup>. At Mach numbers above the critical value the pressure drag is nearly all due to wave drag (the difference being the small pressure out-of-balance caused by the boundary layer), so that changes in lift must be compatible with changes in wave drag. The mechanism which brings about the reduction in wave drag is a consequence of the low pressures in the leading-edge region. The low pressures are associated with expansion waves which leave the surface and then reflect from the sonic line as compression waves. These are augmented by reflection at the aerofoil surface and cause an increase in pressure in a downstream direction, and so reduce the strength of the shock at the end of the supersonic region. By this means there seems to be the possibility of achieving a compression from supersonic to subsonic flow at the trailing edge without a shock wave, or with at most a very weak shock, and eliminating wave drag, as sketched in curve (c) of Fig. 1. The flows on

aerofoils

aerofoils which have been tested at the N.P.L. closely approach this isentropic compression for a range of conditions sufficient to represent significant gains in aircraft performance over what would be otherwise possible, and indicate that such an ideal is a worthwhile design aim. Against this is the possible instability of an isentropic compression to subsonic flow; this question has been considered by, for example, Shapiro<sup>2</sup>, Kuo and Sears<sup>3</sup> and Bers<sup>4</sup>. Mathematical arguments<sup>5</sup> tend to indicate that the ideal cannot be attained but results are still somewhat inconclusive owing to difficulties in formulating the problem. In any case, the presence of a weak shock, although resulting in a breakdown of the isentropic flow in a mathematical sense, would not detract significantly from the performance advantages available to the aircraft designer.

The broad features of the aerofoil geometry required to generate the "peaky", low-pressure region have been outlined by Pearcey in Ref. 1 and more recent, unpublished work at the N.P.L. has gone further in qualitatively describing the necessary shape. It has been found that a rapid change of curvature from a high value at the leading edge to a low value further back is the essential feature. The high curvature from the stagnation point produces a rapid expansion to high, supersonic velocities and the sudden transition to low curvature stops the expansion and determines the "peak" height. The surface shape from then on must be matched to the incoming compression wave to produce the desired pressure distribution.

It has however been found that most aerofoils with satisfactory low pressure "peaks" in the lower transonic range lose their "peaky" behaviour as the free stream is raised towards supersonic speeds if incidence is held constant. In order to investigate further the geometric parameters controlling the form of the low-pressure region and the compression to subsonic flow, the work described in this paper was undertaken using the simplest possible aerofoil shape compatible with the known curvature requirement, namely a circular-arc biconvex aerofoil with a circular, cylindrical blunting of the leading edge. It was not expected that such a shape would be suitable for use in wing design, particularly owing to the boundary-layer separation problems likely to arise at the discontinuous change of curvature for low flight speeds. However, understanding of the flow about such a simple geometric shape should provide information which would enable further developments in "peaky" aerofoil design to be made.

Early tests on this geometry showed that it produced a region of very low pressure in the vicinity of the change of curvature and that this persisted at the high subsonic free-stream speeds. The speed range of interest was then increased to include low supersonic speeds in order to investigate the characteristics of "peaky" aerofoils in this regime.

The basic, sharp leading-edged, biconvex aerofoil was also tested to form a datum from which the effects of leading-edge blunting could be measured.

Factors which affect the application of wind-tunnel data to full-scale, free-flight conditions are the representation of the boundary-layer transition point and tunnel-wall interference effects. The state of the boundary layer would not be expected to affect the surface pressures in an important way providing separation did not occur, so that the main experimental programme was carried out using no artificial means of fixing transition. However, it was found that in some cases a local separation bubble was present near the change of curvature and some limited tests were made on the effects of using a carbomindum strip to promote transition and so suppress the separation. Wall interference in tunnels

similar/

similar to the one used here has been discussed in Ref. 6, where some recommendations for reducing it are made, but little experience is available of the effects that interference has on the pressures in the region of the "1" and of the subsequent compression for aerofoils of the type being considered present, particularly at high subsonic speeds. It was thus found necessary to investigate the effect of varying the slot open-area in order to demonstrate applicability of the experimental data to free-air conditions. This work was only of an exploratory nature and the topic deserves further study.

## 2. Wind Tunnel and Models

The experiments were carried out in an N.P.L. transonic, induced-flow wind tunnel which has a working section measuring 36 in. x 14 in. (91 cm x 36 cm). Slotted top and bottom liners were used in the Mach number range 0.7 to 1.1, solid, supersonic liners for the Mach number of 1.4. The stagnation pressure in this tunnel is limited to just below atmospheric, the small loss being due to gauzes.

Pressures were measured on a multitube, mercury manometer.

The two-dimensional models were mounted spanning the 14 in. width of the tunnel. The basic aerofoil section was circular-arc biconvex, described by radii of 30 in. (76.2 cm) and a chord of 10 in. (25.4 cm), this model being designated R30\*. Blunted sections R3010 and R3015 were derived from the basic sharp shape by leading edges of constant radii 0.10 in. (0.254 cm) and 0.15 in. (0.381 cm) respectively. The leading-edge cylinders blended tangentially with the basic shape, giving chords somewhat less than 10 in. Details of the three section shapes are given in Fig. 2.

The models were made by the "tangent milling" method. In this method the planes are cut tangentially to the required contour, such that the point of intersection of any two adjacent planes deviates from the required shape by 0.0005 in. (0.00127 cm). The final smooth shape is achieved by hand finishing. Static pressure holes were drilled normal to the surface, 0.010 in. (0.0254 cm) diameter generally, but those near the leading edge were made 0.007 in. (0.0178 cm). Forty pressure holes were distributed on the upper and lower surfaces.

## 3. Test Conditions

Surface pressures have been measured and schlieren photographs taken on the sharp and two blunt leading-edged aerofoils over the Mach number range 0.7 to 1.40. In addition, the blunt aerofoils were also tested at a Mach number of 1.40. The incidence range of 0 to 4 degrees was covered at all Mach numbers, except at  $M_0 = 1.40$ , the flow could not be established on the blunt shapes at incidences above about 2 degrees.

The free-stream Reynolds number lay within the range  $3.7$  to  $4.2 \times 10^5$  per in. ( $1.4$  to  $1.6 \times 10^5$  per cm).

The majority of the results were obtained with slotted tunnel-liner open-area ratio ( $\sigma$ ) = 0.091 ( $T = 0.96$ ), and without any artificial means

fixing/

\* The aerofoils referred to here have now been given N.P.L. designations as follows:

R30	:	NPL 9410
R3010	:	NPL 9411
R3015	:	NPL 9412

fixing boundary-layer transition. A limited number of tests were also made under varying conditions, by fixing boundary-layer transition with a leading-edge carborundum strip, and by reducing the liner open-area ratio to 0.025 ( $T = 0.73$ ).

#### 4. Inviscid Flow Behind a Blunt Leading Edge

It will be shown in Section 3.2 that the surface pressures measured on the cylindrical leading edges of aerofoils R3010 and R3015 are in good agreement with those calculated by Chushkin<sup>7</sup> for inviscid flow round a circular cylinder at the same, sonic, free-stream speed. This being established, it is reasonable to assume that Chushkin's solution for the flow field away from the body applies to the aerofoils tested, up to the point where they deviate from a circular shape. It follows that a method is available for calculating the flow field on the aerofoil downstream of the leading edge.

Data along the limiting characteristic, as given by Chushkin, was taken as the initial reference line for a characteristic network. (This limiting characteristic originates from the surface where the slope is 12.5 degrees and the leading edges on aerofoils on R3010 and R3015 terminate where the slopes are 8.4 and 7.7 degrees respectively.) The result of an attempted solution for aerofoil R3015 at  $M_0 = 1.0$  and  $\alpha = 0$  is sketched in Fig. 3(a). It is found that the solution breaks down as soon as the relatively flat surface, AB, is encountered, owing to intersection of characteristics of the family leaving the surface.

In spite of this somewhat negative result the form of the characteristics network does throw some light on the mechanism of the overexpansion and subsequent compression, which is useful in explaining the experimental data. The highly curved surface (SA), following the sonic point (S), generates an expansion wave leaving the surface and a compression wave which approaches the surface, AB, downstream. This compression may be considered as a "reflection" of the expansion at the sonic line. The compression wave then reflects from the aerofoil surface as a further compression wave, the strength of which is governed by the rate of change of surface slope in the region of reflection. In the present case the surface (AB) behind the leading edge is of low curvature, relative to that of SA, and the compression is reflected still as a strong compression wave. The intersection of the characteristics of this compression wave leaving the surface is interpreted as the formation of a shock wave. The flow is analogous to the phenomenon in a compression corner, where a uniform supersonic stream approaches a concave wall (Fig. 3(b)).

It can be seen from the characteristics network that a more highly curved surface, AB, following the same leading edge would allow a compression without intersection of characteristics and, hence, without a shock wave. Alternatively, a flatter surface producing a more rapid rate of compression would give rise to a stronger shock.

The intersection of characteristics following a blunted leading edge on a wedge at supersonic speeds has been previously reported by Chushkin<sup>8</sup>, and he uses this to predict the formation of a shock wave within the flow field. There are other examples in which a shock in the compression following the blunted nose on a cone in supersonic flow has been reported (e.g., Traugott<sup>9</sup>).

The flow field studied here is a particular example of that discussed by Nikolskii and Taganov in Ref. 10. They have investigated the conditions leading to breakdown of potential flow in a local supersonic region and show, in

general/

general terms, that if a surface contour exists to give potential flow then making a segment of the contour flat will cause a shock to form. Moreover, they find that if the contour deformation towards the straight is effected continuously then breakdown of the potential flow will occur before the deformed segment becomes straight. It is this breakdown of potential flow which is shown above as the intersection of characteristics for a surface which is insufficiently curved.

##### 5. Discussion of the Flow about the Aerofoil

Schlieren flow photographs have been obtained for all three aerofoil sections at each value of Mach number and incidence for which pressures were measured. Examples are shown for 2 degrees incidence and Mach numbers of 0.8, 0.9, 1.0 and 1.4 in Figs. 4 and 5, for sections R30 and R3015 respectively. These photographs were taken under conditions of natural transition and a linear open-area ratio of 0.091.

It is seen that the flow on the upper surface, in general, involves shock systems: one emanates from the region just behind the leading edge; the other, which is more common on aerofoils at transonic speeds, lies further back and is required to match the local supersonic flow to the subsonic flow downstream. This latter shock moves aft with increasing free-stream Mach number and lies at the trailing edge for  $M_0 = 1.0$ . At supersonic speeds a further shock appears in the form of the bow shock, seen detached on both the sharp and blunt aerofoils in Figs. 4(d) and 5(d).

On the type of blunt aerofoil considered here the expansion round the leading edge is such that local supersonic flow is reached first in the region of the change of surface curvature (Fig. 5(a)). The flow field at this low end of the transonic range is sketched in Fig. 6(a). In this case a lambda-type of shock formation appears downstream of the change of curvature. The forward leg is an oblique shock embedded within the supersonic flow region and remains at a fixed location, independent of incidence or free-stream speed variations. The downstream leg is approximately normal to the surface and terminates the supersonic region. The latter shock moves downstream with increasing free-stream speed. Also with increasing speed a second region of supersonic flow develops at the region of the crest and is also terminated by a shock wave. This condition is sketched in Fig. 6(b) (see also the pressure distribution for R3010 in Fig. 4). As Mach number is increased still further the two supersonic regions merge to one and the flow is that seen in Fig. 5(b) and sketched in Fig. 6(c); the flow downstream of the first shock system is, at this stage, supersonic. Further increase of Mach number spreads the local, supersonic flow until, for supersonic free-streams, the flow sketched in Fig. 6(d) develops (see also Fig. 5(d)).

The oblique shock-wave system seen just downstream of the leading edge in the schlieren pictures involves a very complex mechanism. The considerations of inviscid flow behind a blunt leading edge in Section 4 indicate that a shock wave caused by the convergence of characteristics, would be present at sonic free-stream speed, and the same process would lead one to expect a shock wave at other transonic speeds. Indeed close examination of some of the schlieren photographs (e.g., Figs. 5(a), (b) and (c)) does show a convergence of weak shocks, growing from near the surface, and coalescing to form a stronger shock well away from the body. In addition the strong, adverse pressure gradient associated with the growth of this shock wave is likely to give rise to separation of the boundary layer, and in some instances the measurements of surface pressure

(see/

(see Section 6.2) do indicate the presence of separation. If the boundary layer is separated then a further shock wave will be caused at its reattachment. Thus there is a mechanism to predict the presence of two shock waves: one accountable from consideration of an inviscid flow; the other arising from viscous effects. These two shocks are likely to become merged and in many cases it would be impossible to say which effect was dominant.

## 6. Pressure Distributions

### 6.1 Results on the sharp aerofoil at $M_0 = 1$ , $\alpha = 0$

The pressure distributions on the sharp leading-edged aerofoil at sonic speed and zero incidence will be considered separately here since it is a case which has received considerable attention in the past. Experimental results are available from the work of, for example, Bryson<sup>11</sup>; Michel, Marchaud and Le Gallo<sup>12</sup>; Henshall and Cash<sup>13</sup> and Kawamura and Karashima<sup>14</sup>. Results from measurements on the sharp aerofoil (R30), with natural transition and a liner open-area ratio of 0.091, are compared with data from some of the above sources in Fig. 7. Pressure is plotted in terms of the reduced pressure coefficient,  $\bar{C}_p$ , of Spreiter and Alksne<sup>15</sup> which, according to the transonic similarity law developed therein, should reduce all the data in Fig. 7, for different thickness-chord ratios, to a single curve. The co-ordinate  $x$  is measured from the leading edges of the aerofoils and is non-dimensionalised by their chords,  $a$ . Also shown is the pressure distribution on a biconvex aerofoil as given by the inviscid theory of Ref. 15. The present results agree quite well with the theory over the forward part of the aerofoil, as do those of Ref. 11 which were obtained on a biconvex fore-body (these are plotted with  $\bar{C}_p - 2\xi_0$  as ordinate since results were only obtained for Mach numbers somewhat different from unity). The large deviation of the results of Ref. 12 near the leading edge is due to the model technique which used a circular-arc bump on a wind tunnel wall, so smoothing out the stagnation point by the wall boundary layer. Over the rearward portions all the experimental results in Fig. 7 show pressure levels below that of the theoretical curve, but the present results are in fair agreement with theory\*. Kawamura and Karashima<sup>14</sup> obtained surface pressures using interferometry techniques and found good agreement with the theory of Ref. 15. (Their results are presented on too small a scale to extract and reproduce here.)

### 6.2 Results on the sharp and blunt aerofoils

In this section the pressure distributions on the sharp and blunt aerofoils will be discussed and compared, with reference to data obtained with natural boundary-layer transition and a liner open-area ratio of 0.091.

Typical examples of the measured upper-surface pressure distributions are plotted for the three aerofoils in Figs. 8 to 12, in order to show the effects of simple, cylindrical blunting of a leading edge (except at  $M_0 = 0.70$ , for which results on R30 were not obtained). The pressure ( $p$ ), non-dimensionalised by the stagnation pressure ( $H_0$ ), is plotted versus the distance ( $x$ ) from the leading edge of the sharp aerofoil, non-dimensionalised by its chord ( $a$ ). The parts of the aerofoils unmodified by blunting are superimposed on the  $x$ -scale, as in Fig. 2.

The/

\* Recent further tests on model R30 in the same tunnel as is used here have shown that better correlation between experiment and theory can be achieved by using less-open tunnel liners. (NPL Aero Report 1168 - "Interference effects at sonic speed for a biconvex aerofoil in a wind tunnel with slotted liners" by W. J. Graham and A. G. J. Macdonald.)

The leading-edge angle of the sharp aerofoil is approximately  $19^\circ$  and is sufficiently large to cause detachment of the bow shock at  $M_0 = 1$  and zero incidence. Therefore the flow about this aerofoil is transonic over the whole Mach number range. At incidence, the stagnation point on the leading edge moves to the lower surface and the flow, in turning round the vanishing small radius to the upper surface, produces a localised region of low pressure as seen in Figs. 9 to 12. (The lower surface pressures are not shown here as there was inadequate detail to locate the stagnation point accurately.) According to the description of a "peaky" aerofoil adopted in this paper (see Introduction), the sharp leading-edged aerofoil exhibits "peaky" behavior.

The pressures on the blunt leading edges of R3010 and R3015, at a free-stream Mach numbers, show an expansive flow occurring on a greatly magnified length scale, compared with the sharp case, and this expansion is also present at zero incidence. Thus, at all incidences and Mach numbers the blunt aerofoils exhibit "peaky" behaviour. The rapid expansion from the stagnation point, the leading-edge cylinder, gives quite high local Mach numbers (e.g., about aerofoil R3015 at  $M_0 = 0.8$ ,  $\alpha = 2^\circ$ ; Fig. 9(a)). This expansion is terminated by the rapid reduction of surface curvature at the junction of the leading-edge cylinder and basic shape. At this stage the flow is over-expanded in the sense that the local pressure is considerably less than that which exists at this point with the sharp leading edge. A compression follows as the pressure moves towards its sharp leading-edge distribution. Sufficiently far downstream the pressures become independent of leading-edge shape.

The mechanism of the compressive flow which immediately follows the expansion round the blunt leading edges has been discussed in Sections 4 and 5 where it is shown that the flow on the present aerofoils always involves a shock-wave system. However, in most cases the pressure distributions in this region are quite smooth, which reinforces the primary explanation developed for the presence of a shock in this region; i.e., the convergence of characteristics to give the growth of a shock away from the surface.

At the lower Mach numbers and incidences the supersonic compression is soon terminated by a shock wave, such as is seen in Fig. 9(a). This shock corresponds to the rear leg of the lambda-type of shock formation seen in the schlieren photograph Fig. 5(a), and it moves downstream with increasing free-stream Mach number or incidence. Also as either Mach number or incidence is increased there is a tendency for the supersonic compression to be followed by an expansion which is then terminated by a shock, as seen in Figs. 9(b) and 10.

For a given geometry, the rate of compression depends on incidence and free-stream Mach number, so that the chordwise extent of the over-expansion is also a function of the same variables. In general terms, for Mach numbers below unity, the chordwise extent of the over-expansion is increased by increasing Mach number (e.g., Figs. 9(a), 10(a) and 11(a)) and incidence (e.g., Figs. 9(b) and 9(b)). For supersonic speeds, the chordwise extent of the over-expansion is decreased by increasing Mach number (e.g., Figs. 11(a) and 12). This is not due to a reversal in the variation of rate of compression with Mach number but instead, caused by the general fall in pressure level on the sharp section itself, so that little compression is needed to return to the sharp section pressure distribution. At sufficiently high supersonic speeds the over-expansion wave is expected to disappear altogether.

The pressure distributions on the two blunt aerofoils show a very similar form throughout the Mach number and incidence range. Apart from a

difference/

difference in leading-edge radius, the two aerofoils have similar geometry (Fig. 2). The aerofoil with the larger leading-edge radius (R3015) has a slightly greater turning angle before the change of curvature and this results in a slightly higher local Mach number in this region than for the other blunt aerofoil (R3010).

At the lower values of incidence and Mach number (see Fig. 8) the region of nearly constant pressure just behind the change of curvature indicates that a local separation of the boundary layer is taking place, as was thought likely in Section 5. Detailed examination of the pressure distributions shows that the pressure gradient ahead of where separation occurs decreases with increasing incidence and Mach number, and at the higher values is evidently insufficient to promote a noticeable boundary-layer separation.

The lower surface pressures are of little interest here. It suffices to say that the region of over-expansion becomes less extensive as incidence is increased, as would be expected from the trends on the upper surface, and that downstream of the over-expansion the pressures are independent of leading-edge geometry, again following the upper-surface behaviour.

### 6.3 Effects of fixing boundary-layer transition

The boundary-layer separation which has been observed in the compression behind the leading edge (Section 6.2) affects the pressures locally, and, in order to investigate this and any additional effects which may occur downstream, some limited tests were made with a 0 to 5% chord, roughness band on upper and lower surfaces. Several densities of carborundum (particle size about 0.002 in. (0.00508 cm)) were tried but the surface pressures were insensitive to this. For this study the liner open-area ratio was retained at 0.091.

A comparison of chordwise pressure distributions with and without roughness is made in Fig. 8(b) for a Mach number of 0.7 and 4 degrees incidence. Without roughness there is a local separation bubble, identified by the region of nearly constant pressure embedded in the compression. With roughness the expansion on the leading-edge cylinder gives lower pressures, and there are no signs of separation in the pressure distribution. The effects of fixing boundary-layer transition at low Mach numbers are shown in greater detail in Fig. 16(a) where the leading-edge pressures are plotted versus the angular co-ordinate  $\bar{\theta}$ . Up to  $\bar{\theta} = 60^\circ$  the state of the boundary layer has no significant effect on the pressures. Beyond this the flow with fixed transition expands to a lower pressure at the pressure minimum ( $\bar{\theta} \approx 65^\circ$ ), and the pressures remain lower than the natural transition values up to the change of curvature ( $\bar{\theta} = 82.3^\circ$  for R3015).

At higher Mach numbers, where no separation is evident in the pressure distribution, the pressures are only slightly affected, at the change of curvature itself, by addition of the roughness band. This is shown on the detailed leading-edge pressure distribution in Fig. 16(b), for  $M_0 = 1.0$ .

It can be concluded that suppression of the separation, by inducing a turbulent boundary layer on the leading edge, does not affect the overall pressure distribution. Thus, we can assume that the observations in this paper are typical of higher, free-flight Reynolds numbers, except in the locality of the separation regions.

## 7. Induced Pressure Differences due to Leading-Edge Blunting

In this Section the pressure differences, between the sharp and blunt aerofoils, are considered as increments induced by the blunt leading edge. The analysis of these increments will be based on the pressure data obtained with natural boundary-layer transition and a liner open-area ratio of 0.091, and presented in Section 6.2.

The turning of the supersonic flow around the leading-edge cylinder produces expansion waves, emanating from the surface, which can be considered to be "reflected" from the sonic line to give a compression wave directed towards the surface (see Section 4). The overall magnitude of this compression wave would be expected to depend on the maximum over-expansion produced at the change of curvature, measured as the difference in pressures at this point for blunt and sharp aerofoils. The compression wave will be modified by the expansive flow produced by the aerofoil shape behind the leading edge, but where the surface curvature is low the compression wave will dominate the flow and produce a net compressive effect. The chordwise extent of the over-expansion, for a given downstream shape, would be expected to depend on the size of the leading edge.

The downstream changes in surface pressure induced by the blunt leading edges are shown in Fig. 13, for all incidences above 0 degrees and at Mach number of one. The zero incidence results which show separation at the shoulder have not been included. The pressure difference,  $\Delta p/H_0$ , is plotted against  $\zeta/a$ , the non-dimensionalised distance measured downstream from the change of curvature.

In order to attempt to achieve a simple correlation, based on the mechanism outlined above, the pressure differences have been non-dimensionalised as the product of  $H_0$  and the appropriate value of  $\Delta p/H_0$  at  $\zeta = 0$  and plotted in Fig. 14 versus the length scale ( $\zeta$ ) non-dimensionalised by the leading-edge radius ( $r$ ). The pressure differences for both blunt leading edges, at a given incidence, are seen to be correlated quite well up to  $\zeta/r = 20$ . However, pressures at the larger values of  $\zeta/r$  ( $> 20$ ) fluctuate considerably. Up to a few leading-edge radii behind the change of curvature, the results for all incidences agree closely, but with increasing distance an effect of incidence becomes evident: the pressure increments approach zero less rapidly as incidence is increased. The expansive flow produced by the surface interacts with and spreads the incoming pressure wave, and as the local Mach number increases, with increasing incidence, this effect becomes more marked.

The correlation of induced pressure differences becomes less good as free-stream Mach number is reduced, but it improves at supersonic speeds. In Fig. 15 are shown the results for incidences from 0 to 2 degrees, at a free-stream Mach number of 1.40, and the correlation is seen to be good. Data obtained by Holder and Chinneck<sup>16</sup>, on a cylindrically-blunted flat plate at a Mach number 1.42, also agrees well with the present data on this basis.

## 8. Flow about the Leading-Edge Cylinders

### 8.1 Pressure distributions

Pressures on the leading-edge cylinders of the blunt aerofoils have been measured in sufficient detail (particularly for aerofoil R3015) to show some interesting effects. In considering the pressures in this region, it should be

borne/

borne in mind that each pressure hole subtends an angle of about 4 degrees for section R3010 and  $2\frac{3}{4}$  degrees for section R3015, and this affects the precision of any analysis. The data considered in this Section was obtained with a liner open-area ratio of 0.091 and with natural transition.

The leading-edge pressures for both aerofoils are plotted versus the angular co-ordinate  $\bar{\theta}$  (measured from the axis of symmetry) in Fig. 16(a), for a free-stream Mach number of 0.7 and zero incidence. The pressures for the two aerofoils are found to be in good agreement. In subsonic flow the pressures at the leading edge are, in principle, dependent on the whole body shape, but the differences in shape between the two aerofoils tested here are evidently insufficient to cause a noticeable effect. Even the pressures on a complete circular cylinder reported by Perkins and Gown<sup>17</sup> are close to those measured here until the change of curvature is approached. In this region the flow on the leading edge is affected by the aerofoil afterbody and a compression starts before the end of the cylinder.

The pressure distributions on the two blunt leading edges are also compared for Mach numbers of 1.0 and 1.4 in Figs. 16(b) and (c) respectively and again are found to be in good agreement. This result is expected for supersonic speeds, when an afterbody does not in theory affect the leading-edge flow. At low supersonic speeds the pressure distribution on a circular cylinder is seen to be well represented by the simple relationship

$$\frac{p}{p_s} = \cos \bar{\theta}$$

up to values of  $\bar{\theta}$  of about 75°. Also shown in Fig. 16(c) are the pressures measured on a cylindrical leading edge on a flat plate at  $M_o = 1.42$ , by Holder and Chinneck<sup>16</sup>. If allowance for the different Mach number is made, their results agree well with the present values. At these high free-stream Mach numbers the flow on the leading edge shows a smooth expansion up to the discontinuity of curvature ( $\bar{\theta} = 82.3$  on section R3015).

The variation of leading-edge pressure with incidence is shown in Figs. 17(a) and (b) for aerofoil R3015 at Mach numbers of 0.8 and 1.0. The stagnation point ( $p/H_o = 1.0$ ) moves round to the lower surface with increasing incidence, the movement being more rapid for the lower Mach number. On the upper surface the local Mach number at a given point increases with incidence, whilst the converse applies on the lower surface. At incidence the pressures on both sections are still in good agreement over most of the leading edge. On the lower surface (negative  $\bar{\theta}$ ) the local Mach number at the shoulder decreases with increasing incidence and eventually becomes subsonic, as seen in Figs. 17(a) and (b). In these circumstances significant afterbody effects are present and agreement between the pressures on the two leading edges in the vicinity of the lower surface change of curvature is not good. The data from aerofoil R3010 is shown with flagged symbols in Fig. 17 where it differs significantly from the R3015 data.

## 8.2 Comparison with theory

The problem of inviscid flow round the forward part of a circular cylinder in a sonic free-stream has been solved numerically by Chushkin<sup>7</sup> using Dorodnitsyn's method of integral relations<sup>18</sup>. These theoretical surface

pressures/

pressures are compared with those measured on the present leading-edge cylinder in Fig. 16(b) and are in good agreement.

According to the theoretical solution the limiting characteristic leaves the leading edge where the surface slope is about  $12.5$  degrees and changes in the body shape behind this point will not affect the upstream flow, provided the disturbances due to the changes still allow isentropic flow. For the aerofoils tested here it has been shown in Sections 4 and 5 that the body shape generates a shock wave just behind the leading-edge cylinder and this might be expected to show some effect on the leading-edge flow field. However, the agreement between experiment and theory indicates that for these aerofoils, at zero incidence, the afterbody shape is having no appreciable effect on the leading-edge surface pressures.

### 8.3 Movement of stagnation point

It is observed from plots such as those shown in Figs. 17(a) and (b) that the pressure distributions retain their general form as incidence is varied, the effect of incidence being mainly to shift the distribution through an angle amount equal to the shift of the stagnation point. This result would be expected at supersonic Mach numbers for a cylindrical leading edge, since the limiting characteristics would then always lie on the cylindrical part and the body shape forward of them would remain unchanged with incidence.

In an attempt to correlate the angular displacement of the pressure distributions with incidence a new angular co-ordinate  $\bar{\theta} + k\alpha$  has been used where  $k$  has been chosen to achieve a "best correlation" of pressures for all incidences at a given Mach number. Typical cases for Mach numbers of  $0.8$  and  $1.0$  are shown in Figs. 18(a) and (b), for which  $k$  is chosen as  $3.5$  and  $2.0$  respectively. The correlation achieved is very good, except for regions close to the lower surface shoulder, where the local speed becomes subsonic at high incidence, and for regions close to the upper surface shoulder at low incidence.

The variation of  $k$  with Mach number is shown in Fig. 19, where results for both aerofoils agree within the limits of the uncertainty indicated. The parameter  $k$  (the rate of movement of stagnation point with incidence) is found to decrease with increasing Mach number. It is expected that  $k$  should tend to unity for sufficiently large, supersonic speeds, since the limiting characteristics move forward with increasing Mach number and the afterbody shape has less chance of influencing the upstream flow.

### 8.4 Movement of sonic point

The measured pressure distributions can be used to find the sonic point on the leading-edge cylinder, its position being defined by  $p/H_0 = 0.528$ . The variation of sonic point position given by its angular co-ordinate,  $\bar{\theta}^*$ , is shown as a function of Mach number in Fig. 20, for various incidences.

At zero incidence the forward movement of the sonic point ( $\bar{\theta}^*$  decreases) is simply due to the general increase in surface Mach number as the free-stream Mach number increases. When at incidence, however, the movement of the sonic point with increasing Mach number is the resultant of two contributions: one tends to move the sonic point forward, just as at zero incidence, while the other is due to the forward movement of the stagnation point on the lower surface which tends to move the sonic point aft. At  $2$  degrees incidence and above, the latter effect dominates to give the net rearward movement with Mach number seen in Fig. 20.

Since, /

Since, at zero incidence, the sonic point moves forward with increasing Mach number, so that there is more supersonic expansion before the change of curvature, the peak Mach number increases with free-stream Mach number. At incidences of 2 degrees and above, the peak Mach number will decrease with increasing free-stream Mach number, because of the rearward movement of the sonic point and the decrease of turning angle before the change of curvature. These variations of peak Mach number are seen by comparing Figs. 17(a) and (b). It is this sonic point movement which has caused the "peak" to disappear at Mach numbers approaching one on many aerofoils which have been developed at the N.P.L. to have moderate "peak" heights at lower speeds. On these, the change of curvature occurs at a lower value of  $\theta$  so that, at high Mach numbers, there is insufficient supersonic expansion between the sonic point and shoulder to produce a significant "peak".\*

#### 9. Lift Coefficients and Lift-Drag Ratios

Lift coefficients have been obtained by integration of the measured pressure distributions using the relationship

$$C_L = \int_0^1 \Delta C_P d\left(\frac{x}{c}\right) = \frac{2H_0}{\gamma P_0 M_0^2} \int_0^1 \Delta \left(\frac{P}{H_0}\right) d\left(\frac{x}{c}\right),$$

where ' $\Delta$ ' denotes the difference between upper and lower-surface values.

The variation of lift coefficient with Mach number is shown in Fig. 21 for the blunt aerofoil R3010 at 2, 3 and 4 degrees incidence. Curves have been drawn only for this aerofoil, for which data at  $M_0 = 0.85$  has been obtained, and these are shown dotted where uncertainty remains as to their exact form. The variation of lift coefficient with Mach number is typical of that for general aerofoils with shock-induced separation in the transonic range. At a given incidence, lift increases to a maximum at a Mach number of about 0.85 and then falls rapidly with increasing Mach number up to about 0.9, beyond which it rises to a second maximum near 1.05 Mach number. Lift coefficient then falls slowly with increasing supersonic speed.

The variation of lift with incidence is shown for all three aerofoils in Figs. 22(a), (b) and (c) at Mach numbers of 0.8, 1.0 and 1.4 respectively. At all incidences for the lower Mach numbers (Figs. 22(a) and (b)) the lift coefficient is increased by blunting the leading edge. This effect is due to the low pressure region, induced by the leading-edge bluntness, which was discussed in Sections 6.2 and 7. The chordwise extent of the over-expansion increases with increasing leading-edge radius and, correspondingly, the lift coefficient increases at the same time. The changes in lift at the higher Mach numbers are less marked because the extent of the over-expansion decreases with increasing supersonic speed, as was noted in Section 6.2. At the Mach number of 1.4, lift coefficient is not appreciably altered by leading-edge blunting (Fig. 22(c)).

The pressure-drag coefficients for these aerofoils are discussed in detail in Ref. 19. These drags were obtained by integration of the measured

surface/

---

\* The results of the tests on the circular leading edges show that the height of the pressure "peak" will always tend to decrease with increasing Mach number. However, it is quite possible for an aerofoil to have a satisfactory "peak" height at low speeds but still generate a significant "peak" at near-sonic speeds.

surface pressures and the results at Mach numbers of one and above have been "corrected" to remove boundary-layer shock-wave interaction effects at the trailing edge. The lift-drag ratios for all three aerofoils have been calculated and are shown in Figs. 23(a), (b) and (c) for Mach numbers of 0.8, 1.0 and 1.4 respectively. At the lowest Mach number the effect of blunting leading edge is to increase the lift-drag ratio, except for section R3015 at highest incidences (Fig. 23(a)). However, lift-drag ratio does not progress increase with leading-edge radius and aerofoil R3010 has higher values than R3015 this being due to the higher drag of the latter section. At sonic free-stream speed (Fig. 23(b)) the blunt aerofoils have higher lift-drag ratios only at low incidences and again the aerofoil R3010 has higher values than aerofoil R3015. At the supersonic Mach number of 1.4 the lift-drag ratio is progressively reduced by blunting at all incidences (Fig. 23(c)).

The comparison of lift-drag ratios made so far is between aerofoils with different thickness-chord ratios, as the blunting for the present series aerofoils has been effected by cutting back the leading edge and thus increasing the thickness-chord ratio. A more valid comparison of performance of sharp blunt aerofoils would be made by comparing shapes of the same thickness-chord ratio. This can be done using the present sharp aerofoil data and applying transonic similarity law of Ref. 15 to the measured force coefficients to obtain data appropriate to sections of different thicknesses. According to the transonic similarity law, the lift-drag ratio of a section of thickness  $\tau_1$ , at a Mach number  $M_{O1}$ , is related to the lift-drag ratio of a section of thickness  $\tau_2$ , at a Mach number  $M_{O2}$ , by

$$\left( \frac{C_L}{C_D} \right)_1 \cdot \tau_1 = \left( \frac{C_L}{C_D} \right)_2 \cdot \tau_2,$$

where  $M_{O1}$  and  $M_{O2}$  are related through the similarity parameter

$$\xi_0 = \frac{1 - M_{O1}^2}{[(\gamma+1) \tau_1 M_{O1}^2]^{2/3}} = \frac{1 - M_{O2}^2}{[(\gamma+1) \tau_2 M_{O2}^2]^{2/3}}.$$

The lift-drag ratios of a sharp aerofoil of thickness-chord ratio equal to that of the blunt aerofoil R3015 ( $\tau = 0.092$ ) have been calculated by this procedure and are shown in Fig. 23. Except for the Mach number of unity these lift-drag ratios apply at slightly different Mach numbers to those for which the measured values apply, the actual values being indicated in Figs. 2 and (c). The sharp aerofoil is seen to have lower values of lift-drag ratio than the blunt aerofoil at Mach numbers of 0.8 and 1.0, but slightly higher values at the supersonic Mach number of 1.4.

#### 10. Effects of Tunnel-Wall Interference

The results at the Mach number of 1.4 are free from any tunnel interference effects since the model lies within the diamond formed by the bow shock and its reflection from the walls. At the very low supersonic speeds local pressures are "frozen" (i.e., nearly independent of free-stream Mach number) and therefore not greatly affected by tunnel interference, the main influence in this case being to alter the effective free-stream Mach number.

At/

At subsonic speeds the results would be subject to significant tunnel interference effects due to both classical blockage and lift-interference, the latter being predominantly due to the downwash effects appropriate to an open-jet configuration.

In the transonic speed range, between these two regimes, a mixture of the two situations occurs. In the local supersonic flow upstream of the shocks the local pressures tend to be uninfluenced by the walls, especially when they have reached their sonic-range "freeze" values. In the subsonic flow downstream, however, the blockage effects, at least, still apply and particularly the position of the terminating shock is still influenced by the wall configuration.

In Ref. 6, Pearcey, Sinnott and Osborne considered these interference effects and drew attention to a local distortion of the local supersonic flow that could occur prior to the sonic "freeze", if the open area of the slotted liners is too large. Their main discussion concerns measurements in an N.P.L. 20 in. x 8 in. (50.8 cm x 20.3 cm) working-section tunnel, but some results are included for the 36 in. x 14 in. tunnel used here. The liners normally used in this tunnel are 0.091 open-area ratio and give effectively "open-jet" blockage correction. The slotted-wall parameter,  $T$ , of Meader and Wood<sup>20</sup> equals 0.96 in this case (see table in Fig. 24). This parameter involves slot spacing, tunnel height and open-area ratio and defines the wall characteristics explicitly. According to Ref. 6, closing all but three of the eleven slots in each liner gives nearly zero interference liners ( $\sigma = 0.025$ ,  $T = 0.73$ ). The more open liners are normally used since they allow operation up to higher free-stream Mach number.

In order to obtain some measure of the importance of tunnel interference effects in the present cases, limited tests were carried out using models R30 and R3015 with a liner open-area ratio of 0.025. The maximum Mach number attainable with the liner slots in this partially closed position was about 0.9. The variations of pressure with free-stream Mach number for points at the over-expansion at the shoulder and at about 44% chord have been discussed in Ref. 19. There it was shown that the pressures in the over-expansion "freeze" at a Mach number of about 0.8, whereas further back on the chord the pressures "freeze" at a Mach number of about 0.9. As expected, the local pressures are little affected by wall interference at Mach numbers above those at which the onset of sonic "freeze" occurs.

The effect on the chordwise pressure distribution of varying the liner open-area ratio is shown in Fig. 24, for aerofoil R3015 at 2 degrees incidence. The comparisons are made by comparing pressures obtained for different liner configurations but the same free-stream Mach number, as indicated by an upstream, wall static-pressure orifice. At a Mach number of 0.7 (Fig. 24(a)) there is a small reduction in pressure, over most of the upper and lower surface, brought about by reducing the open area. At the higher Mach number of 0.8 (Fig. 24(b)) the pressures near the leading edge, on the upper surface, are "frozen" but further back there is a marked effect associated with the movement of the shock wave from 10% to 60% chord. Where the flow is locally subsonic, at  $M_0 = 0.8$ , the effects of changing wall configuration are similar to those at  $M_0 = 0.7$ . At the Mach number of 0.9 the pressures ahead of the shock wave are "frozen", but again there is a pronounced effect of liner open-area on shock position for both upper and lower-surface shocks. Tests on aerofoil R30 show similar effects brought about by reducing the open-area ratio from 0.091 to 0.025.

If the leading-edge pressures are plotted versus the angular co-ordinate  $\bar{\theta}$  (as in Section 8.1) for the two values of liner open-area, it is found that the

position/

position of the stagnation point moves aft on the lower surface as the open area is reduced. However, the changes are small and involve movements of stagnation point of approximately 1.5 to 1.0 degrees for Mach numbers of 0.7 and 0.8 respectively. Any change in the stagnation point position is not discernable at  $M_0 = 0.9$ . If the rate of change of stagnation point position with incidence established in Section 8.3 is assumed to apply, then the effective change of incidence is a 0.3 degrees for Mach numbers of 0.7 and 0.8, and zero for higher speeds. This shows that the classical tunnel-correction to incidence ceases to apply as sonic speed is approached, and that the actual correction to incidence decreases with increasing Mach number to become zero when the leading-edge pressures have "fro". The changes of linear open-area are accompanied by changes in corrected tunnel Mach number, so that a slightly different value of  $k$  should be used for each value of linear open-area ratio. However, these effects are small (since the changes in corrected tunnel Mach number at  $M_0 = 0.7$  and  $M_0 = 0.8$  would be only about 0.01 and 0.02 respectively) and would not alter the above figures for the change of effective incidence.

A considerable amount of experimental work would be necessary to arrive at the corrections needed to apply the present data to free-air conditions. However, the comparisons made here between the three aerofoil sections involve changes in the flow at the leading edge and over the forward parts of the aerofoils, and this region is little affected by tunnel interference at Mach numbers above 0.8. The main effect of tunnel interference thereafter is to alter the position of the rear shock and thus the absolute magnitude of the force coefficients.

## 11. Conclusions

The geometrically simple, blunt aerofoils considered here show a "peak" type of behaviour throughout the transonic and low-supersonic speed range, and at incidences up to 4 degrees. The supersonic compression from the "peak" involves a shock wave which is shown to be due, primarily, to the intersection of characteristics of the family leaving the surface behind the leading edge. In many cases it is probable that, if the boundary layer is laminar, the strong adverse pressure gradient in this region also separates the boundary layer and gives rise to another shock at reattachment. The two shocks merge together and cannot be separately identified in the experimental observations.

Comparisons between the data for the blunt aerofoils and the sharp, biconvex aerofoil show that the chordwise extent of the low-pressure region, induced by the blunting, increases with leading-edge radius, but that the effects of blunting decay rapidly in a downstream direction. Thus the leading edge is not very effective in modifying the pressures, and therefore shock strength, in the vicinity of mid-chord, in spite of the very large leading-edge radii used here.

The pressures on the leading-edge cylinders are found to be insensitive to afterbody shape even at subsonic free-stream speeds. Analysis of the leading-edge pressure distributions shows that the angular movement of the stagnation point is proportional to the angle of incidence. The constant of proportionality decreases from about 5 at  $M_0 = 0.7$  to 2 at  $M_0 = 1.0$ , and becomes equal to its expected supersonic value of unity at  $M_0 = 1.4$ . The

sonic/

-----  
\* It may be that for some other aerofoils, which do not give a shock in the supersonic compression, the downstream influence of the leading edge is more than that found here. However, it has been noticed in aerofoil design work that ad hoc variations of leading-geometry are often ineffective in producing variations in surface pressure downstream of the leading-edge region.

sonic point on the blunt leading edge moves forward with increasing Mach number when the aerofoils are at zero incidence. However, at moderate incidences the sonic point is found to move rapidly rearwards on the leading-edge radius as sonic free-stream speed is approached.

The low pressures induced on the aerofoil upper-surface by the blunt leading edges are effective in increasing the lift coefficient, and the lift coefficient increases with leading-edge radius. These effects are most marked at subsonic speeds and decrease with increasing Mach number to become insignificant at  $M_0 = 1.4$ .

At subsonic speeds the blunt aerofoils show higher lift-drag ratios than the sharp aerofoil, but the lift-drag ratio does not increase uniformly with increasing leading-edge radius. At  $M_0 = 1.0$  the effect of blunting depends on the angle of incidence. At  $M_0 = 1.4$  the lift-drag ratio is less for the blunt aerofoil than for the sharp one. However, if a comparison is made between measured lift-drag ratios for the blunt aerofoils and estimated values for sharp sections of the same thickness-chord ratios, it is found that leading-edge blunting increases lift-drag ratio for all incidences and Mach numbers up to values just in excess of unity. At  $M_0 = 1.4$  the effect of blunting is still to reduce lift-drag ratio.

#### Acknowledgements

Acknowledgement is due to Miss B. Redstone, Miss A. G. Macdonald and Mr. P. Squire for carrying out most of the experimental work and, together with Miss S. Woolgar and Miss J. A. Soulsby, assisting with the data reduction. Mr. K. Watson and Mr. J. Parker made the wind-tunnel models.

---

#### References/

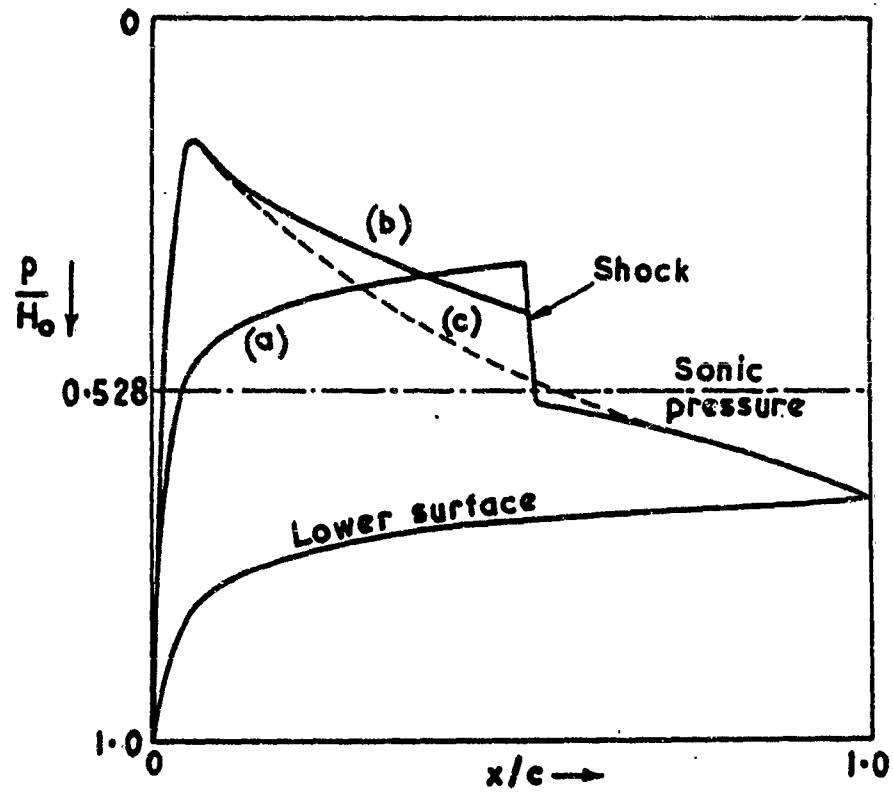
References

<u>No.</u>	<u>Author(s)</u>	<u>Title, etc.</u>
1	H. H. Pearcey	The aerodynamic design of section shape for swept wings. Advances in Aeronautical Sciences, 1 p.277. Pergamon Press, 1962.
2	A. H. Shapiro	The dynamics and thermodynamics of compressible fluid flow. Vol.II, pp.896 and 889. The Ronald. 1954.
3	Y. H. Kuo and W. R. Sears	The general theory of high speed aerodynamics. Vol.VI, p.561. Ed. W. R. Sears. Oxford University 1955.
4	L. Bers	Mathematical aspects of subsonic and gasdynamics. Vol.3. Of surveys in mathematics. p.112. John Wiley & Sons, Inc. 1958.
5	C. S. Morawetz	On the non-existence of continuous trans flows past profiles. I. Comm. on F Applied Maths., Vol.9, pp.45-68, 1955
6	H. H. Pearcey, C. S. Sinnott and J. Osborne	Some effects of wind tunnel interference observed in tests on two-dimensional aerofoils at high subsonic and trans speeds. AGARD Report 296, 1959.
7	P. I. Chushkin	Calculation of certain sonic flows of R.A.E. Library Translation 816, 1959.
8	P. I. Chushkin	Supersonic flows around blunted bodies simple shape. P.M.M., Vol.24, No.5, pp.1397-1403,
9	S. C. Traugott	An approximate solution of the direct supersonic blunt-body problem for axisymmetric shapes. J. of Aero. Sciences, Vol.27, No.5, pp.361-370, 1960.
10	A. A. Nikolskii and G. I. Taganov	Gas motion in a local supersonic region conditions of potential flow breakdown NACA TM 1213, 1949.
11	A. E. Bryson	An experimental investigation of trans flow past two-dimensional wedge and circular-arc sections using a Mach-Zehnder interferometer. NACA Report 1094, 1952.

<u>No.</u>	<u>Author(s)</u>	<u>Title, etc.</u>
12	R. Michel, F. Marchaud and J. Le Gallo	Etude des écoulements transoniques autour des profils lenticulaire, a incidence nulle. ONERA Report 65, 1953.
13	B. D. Henshall and R. F. Cash	Observations of the flow over a two-dimensional 4% thick biconvex aerofoil at transonic speeds. A.R.C. 20 654 - F.M.2765. 2nd January, 1959.
14	R. Kawamura and K. Karashima	Experimental investigation of transonic flow past two-dimensional biconvex circular-arc airfoils at small angles of attack. Aeronautical Research Institute, University of Tokyo, Report 342, 1959.
15	J. R. Spreiter and A. Y. Alksne	Thin airfoil theory based on approximate solution of the transonic flow equation. NACA TN 3970, 1957.
16	D. W. Holder and A. Chinneck	The flow past elliptic-nosed cylinders and bodies of revolution in supersonic air streams. Aeronautical Quarterly, Vol.IV, 1954.
17	F. E. Gowen and E. W. Perkins	Drag of circular cylinders for a wide range of Reynolds numbers and Mach numbers. NACA TN 2960, 1952.
18	A. A. Dorodnitsyn	A method for the numerical solution of certain non-linear problems of aero- hydrodynamics. Transactions of the 3rd All-Union Mathematical Conference, Vol.2, 1956.
19	W. J. Graham	The pressure drag due to blunt leading edges on two-dimensional aerofoils, at transonic and low-supersonic speeds. NPL Aero Report 1151. A.R.C.26 955 - Perf.2403 - F.M.3604 - P.A.1137. 19th May, 1961.
20	P. F. Maeder and A. D. Wood	Transonic wind tunnel test sections, ZAMP., Vol.7, No.12, 1956.

27 838

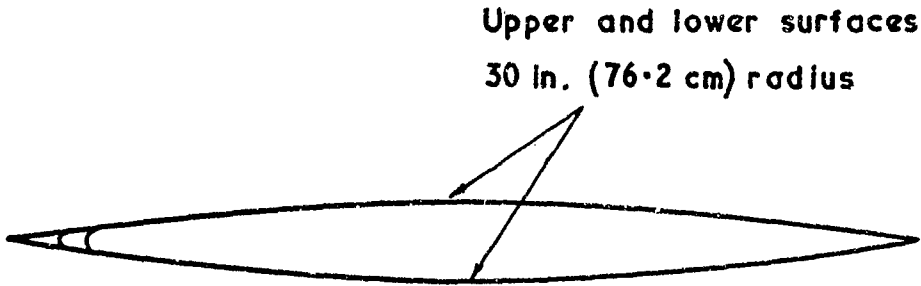
FIG. 1



Sketched pressure distributions for "peaky" and "non-peaky"  
types of aerofoils

- (a) "Non peaky"
- (b) "Peak" (partial isentropic compression)
- (c) Ideal "peaky" (with completely isentropic compression)

**27 838**  
**FIG. 2**

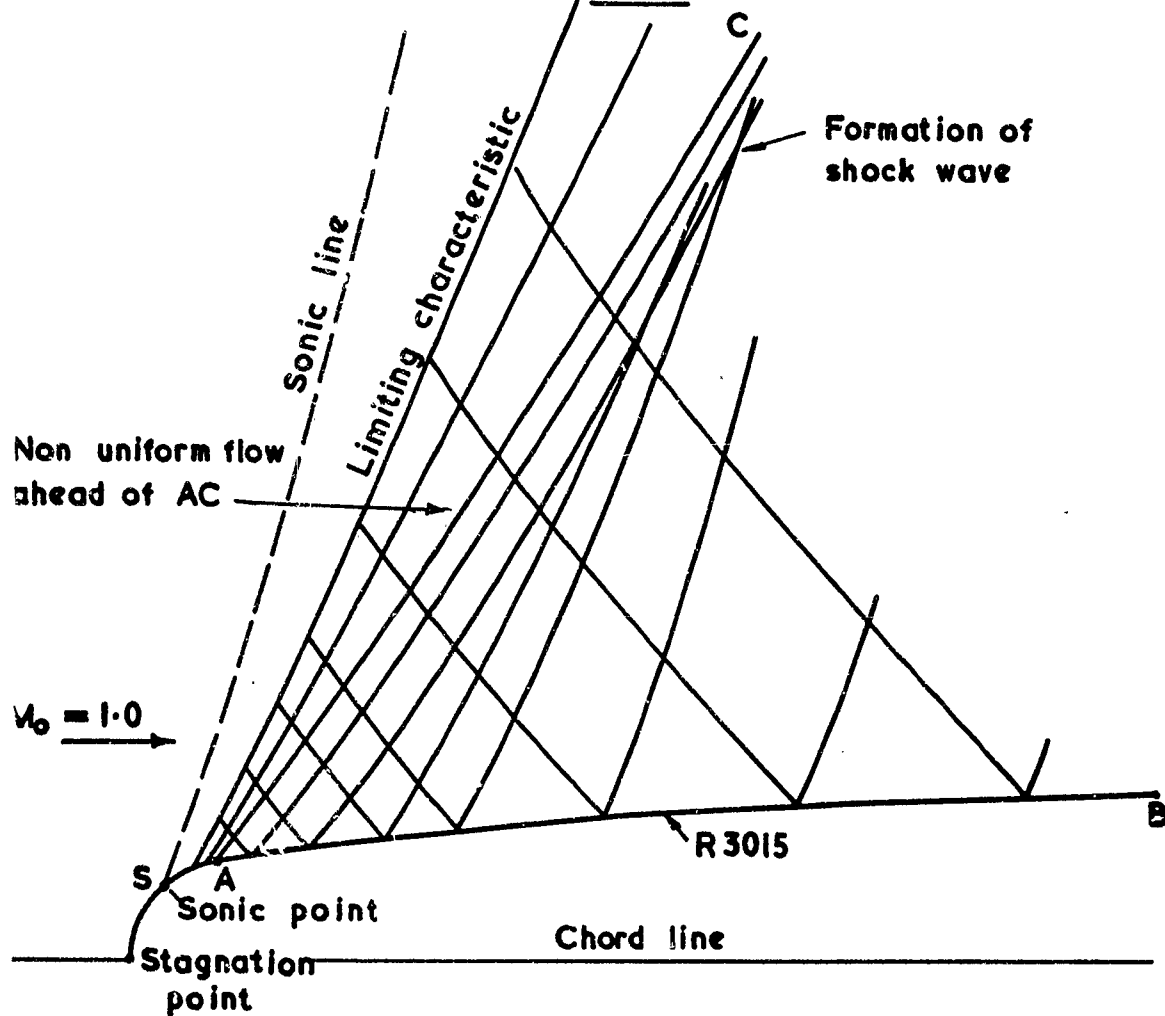


Model designation	L.E. Radius		Chord		Thickness- chord ratio
	in.	cm	in.	cm	
R 30	0	0	10.00	25.4	0.0839
R 3010	0.10	0.254	9.46	24.0	0.0887
R 3015	0.15	0.381	9.15	23.2	0.0917

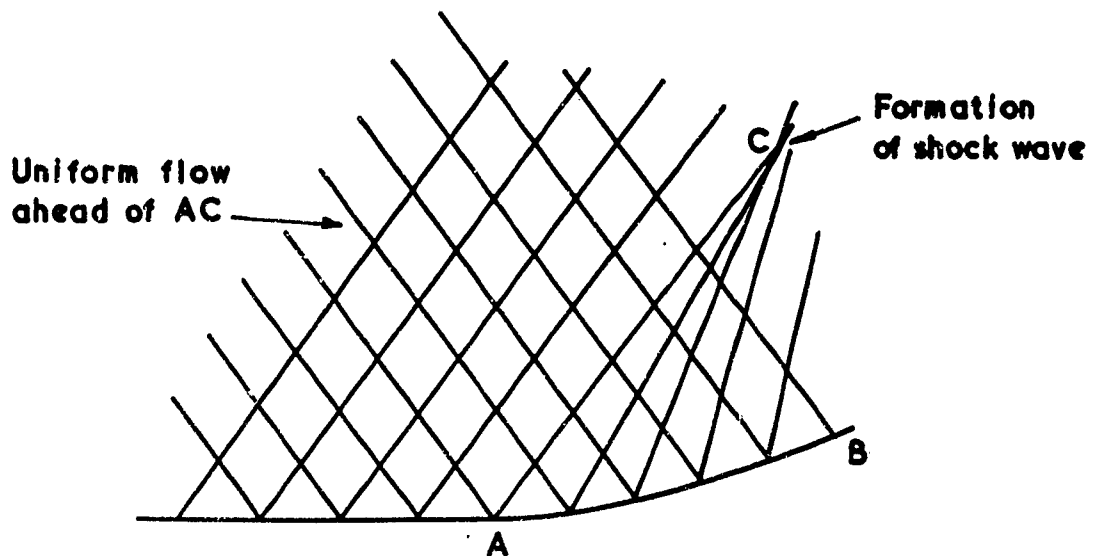
Description of aerofoil sections for two-dimensional models

27 838

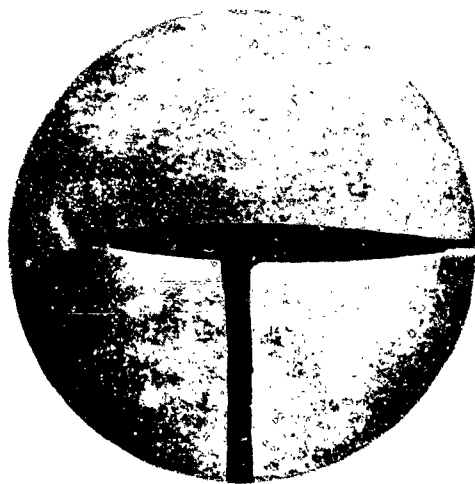
FIG. 3



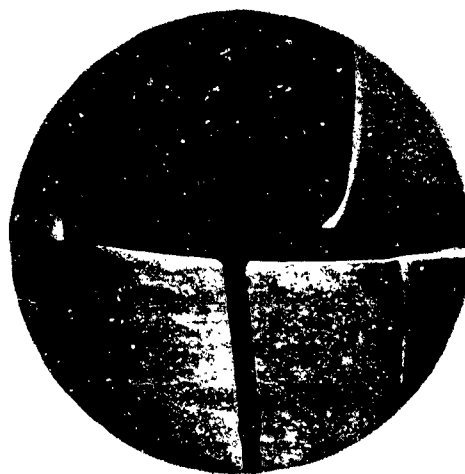
- a) Sketched characteristics solution on aerofoil R3015,  $\alpha = 0^\circ$ ,  $M_0 = 1.0$   
 (Non-uniform supersonic flow approaching convex surface AB)



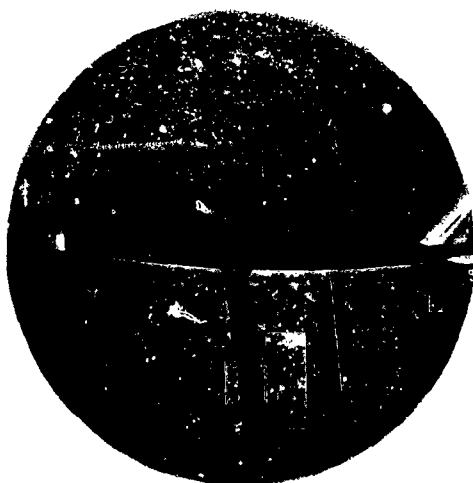
- b) Sketched characteristics solution on a compression corner  
 (Uniform supersonic flow approaching concave surface AB)



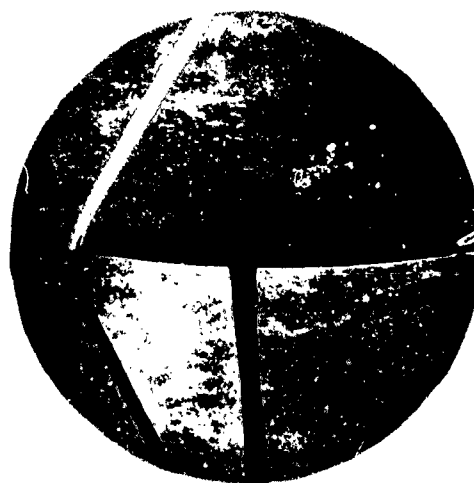
(a)  $M_o = 0.80$



(b)  $M_o = 0.90$

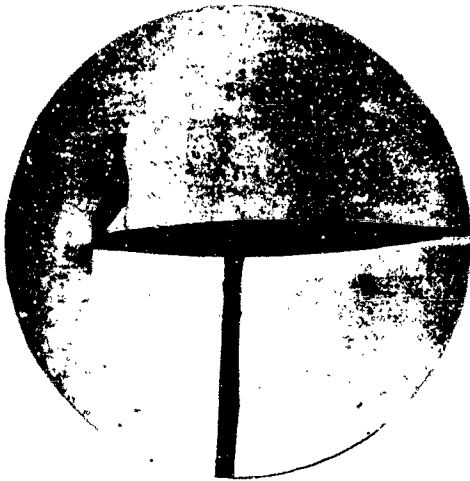


(c)  $M_o = 1.00$

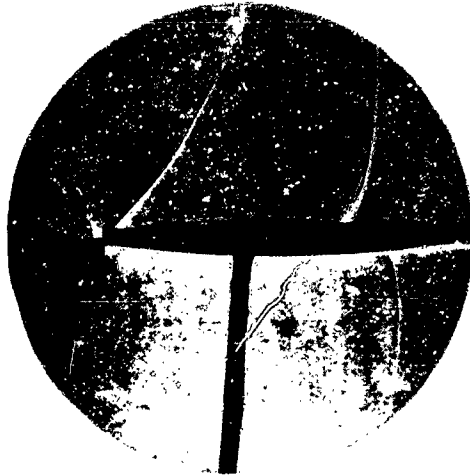


(d)  $M_o = 1.40$

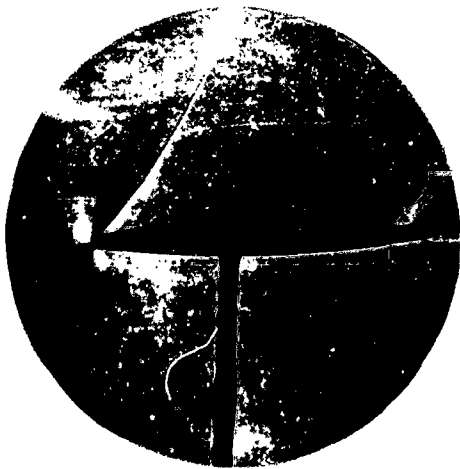
Schlieren photographs of flow over aerofoil R30,  $\alpha = 2^\circ$



(a)  $M_o = 0.80$



(b)  $M_o = 0.90$



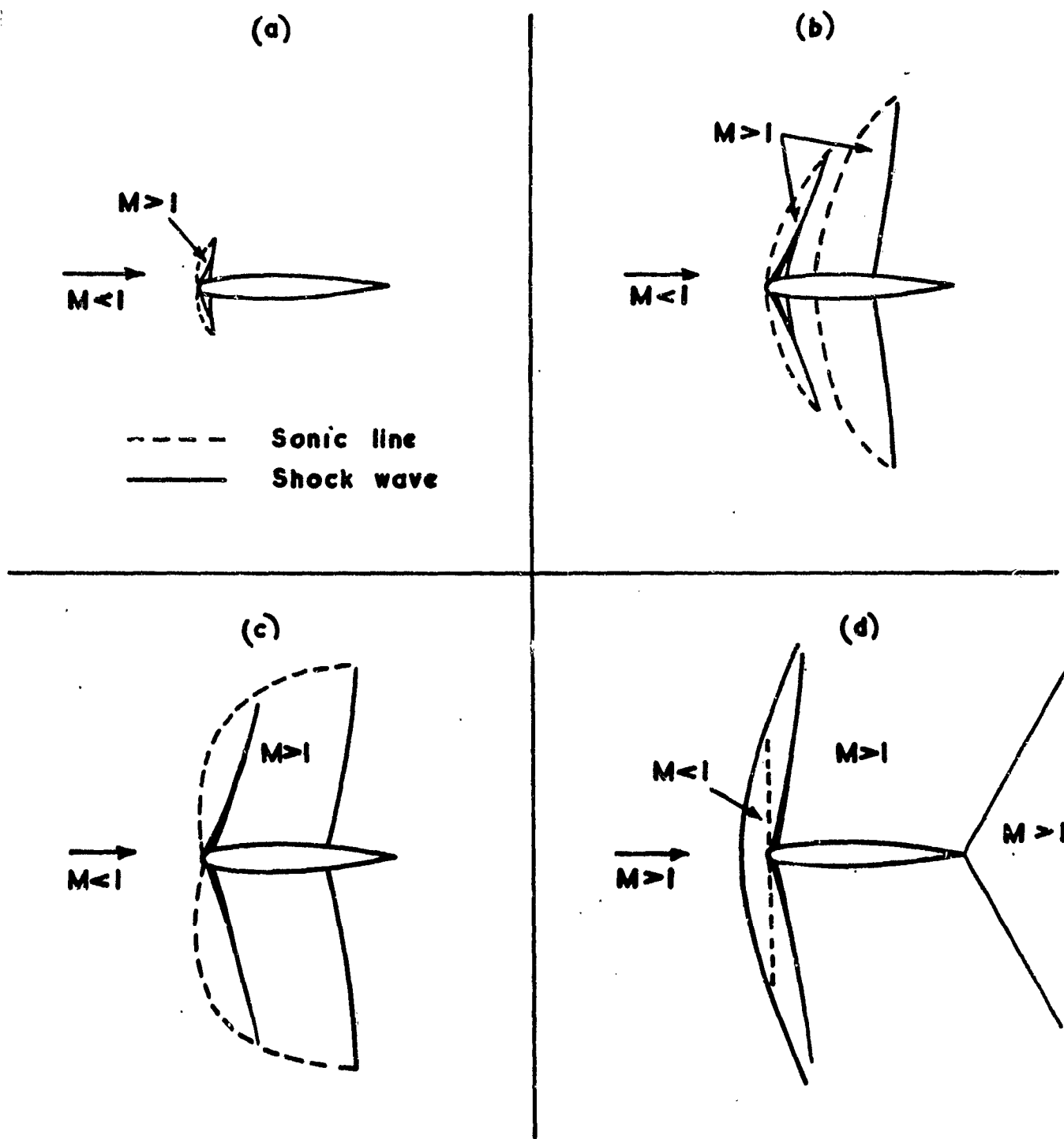
(c)  $M_o = 1.00$



(d)  $M_o = 1.40$

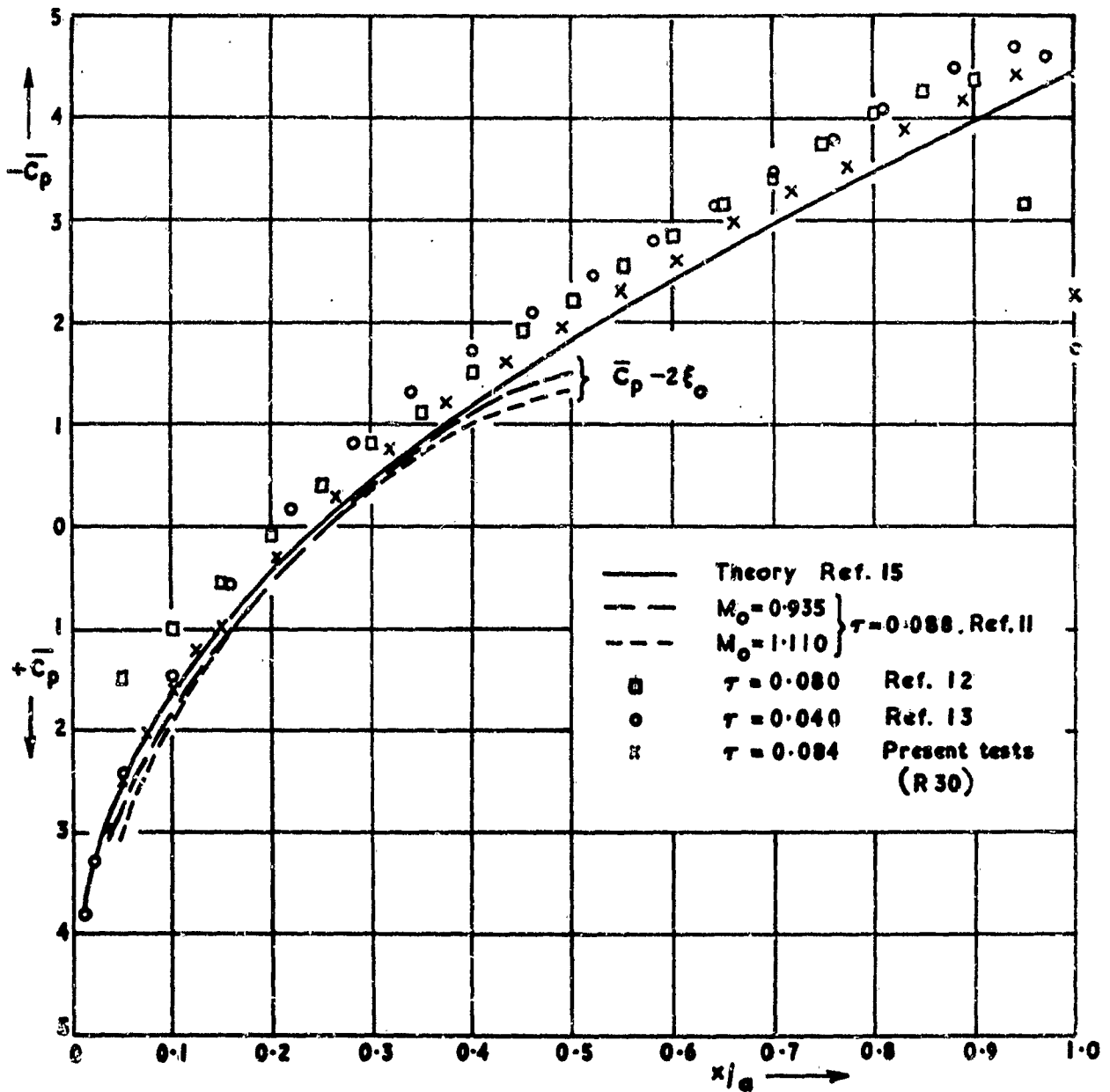
Schlieren photographs of flow over aerofoil R3015,  $\alpha = 2^\circ$

**27838**  
**FIG. 6**



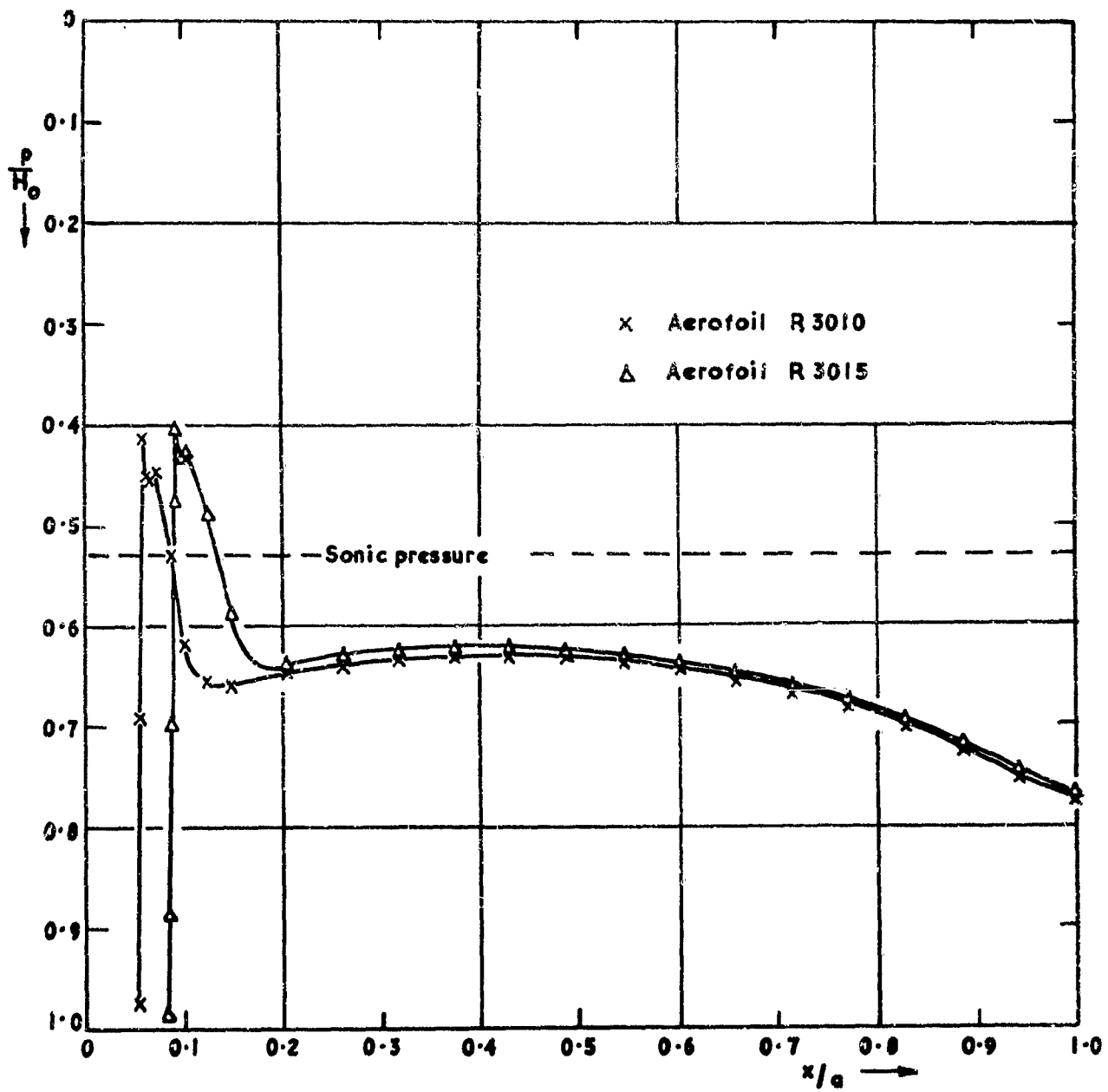
**Sketched transonic flow fields about the blunt leading-edged**  
**aerofoils at increasing free-stream Mach numbers**

27838  
FIG. 7



Comparison of pressures on circular-arc biconvex aerofails at  $M_0 = 1.0$ .  
 $\alpha = 0^\circ$

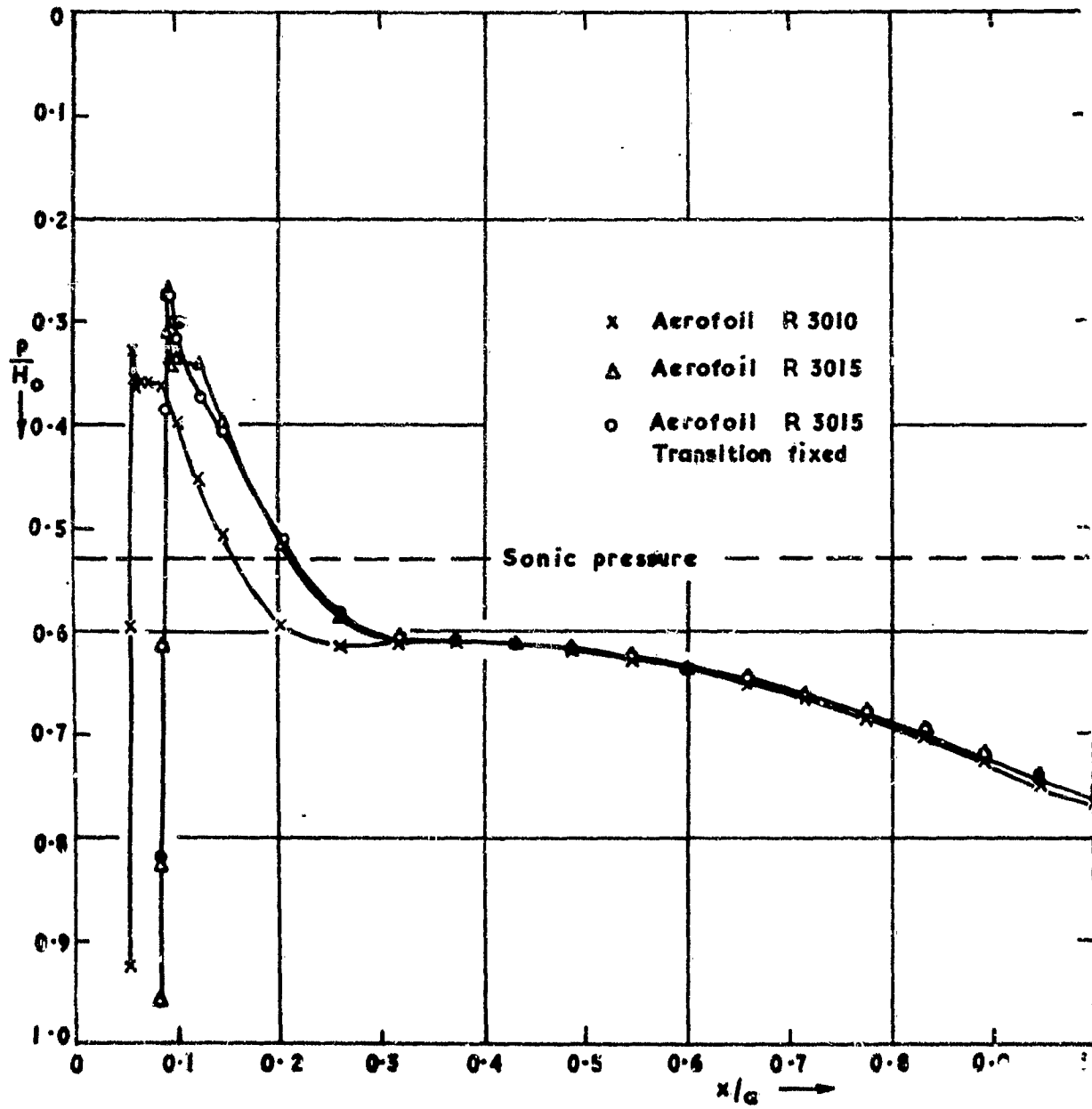
27838  
FIG. 8 (a)



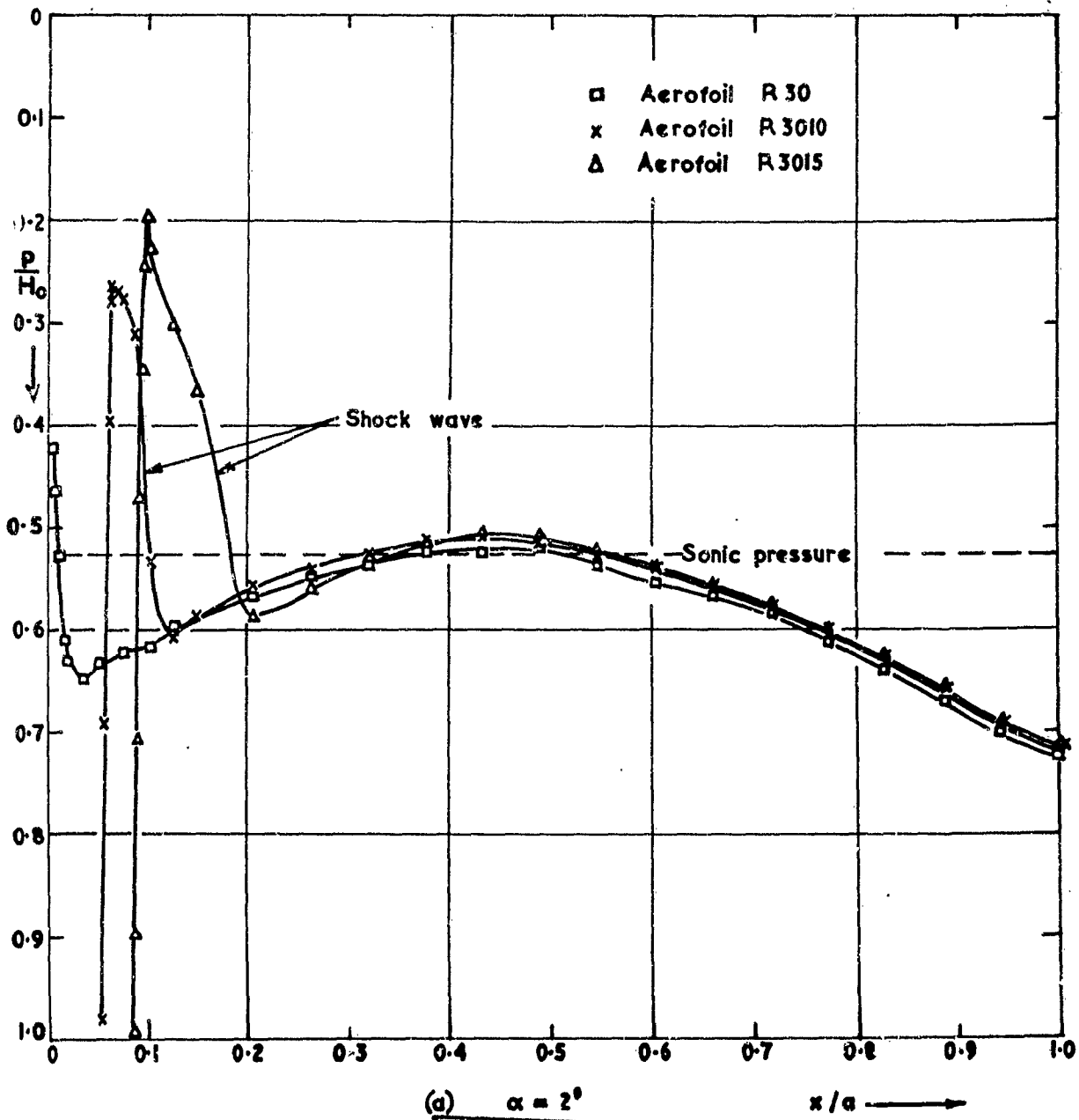
(a)  $\alpha = 2^\circ$

Comparison of upper-surface pressures on the blunt leading-edged aerofoils at  
 $M_0 = 0.70$

27838  
FIG. 8 (b)

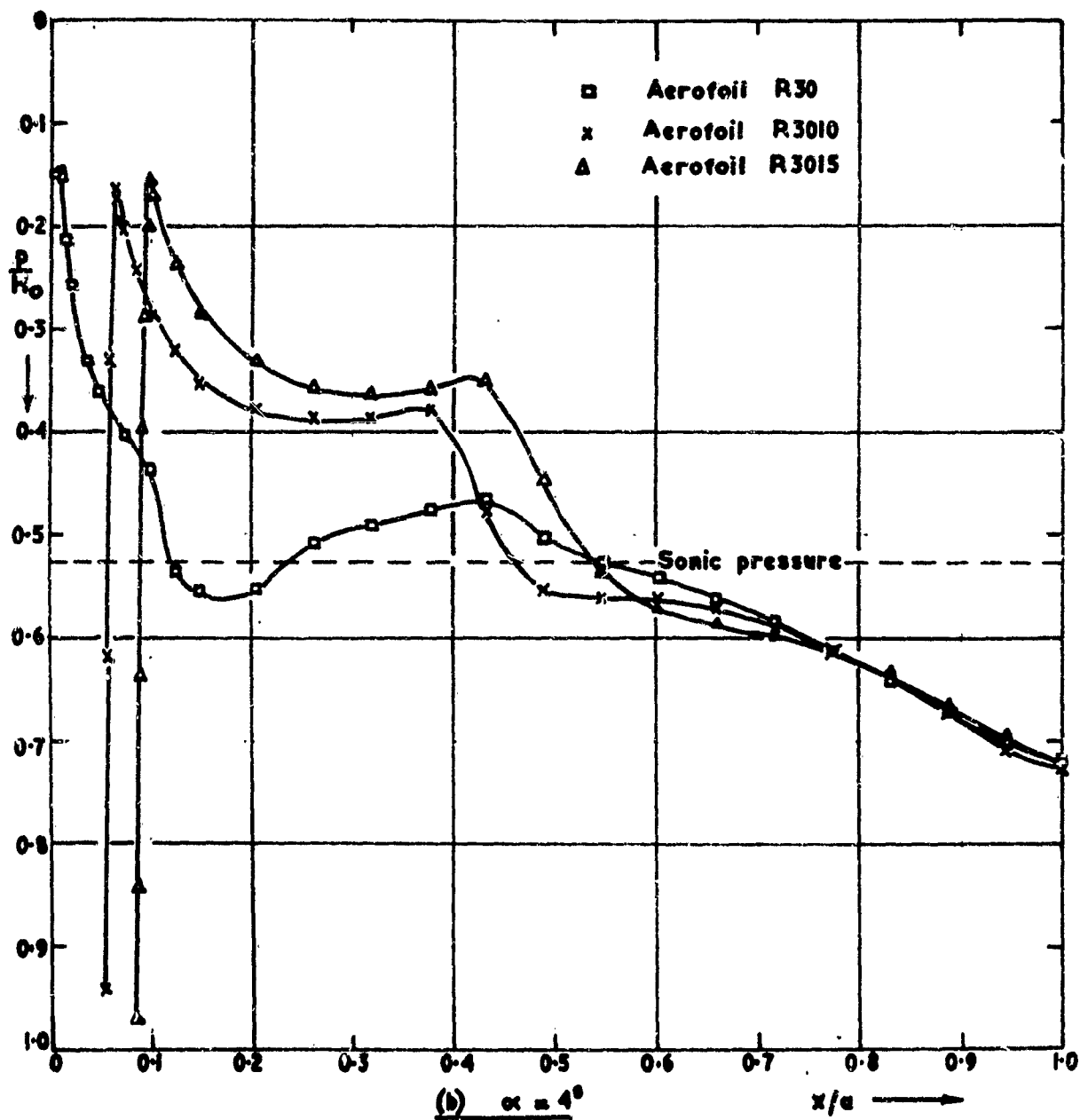


(b)  $\alpha = 4^\circ$

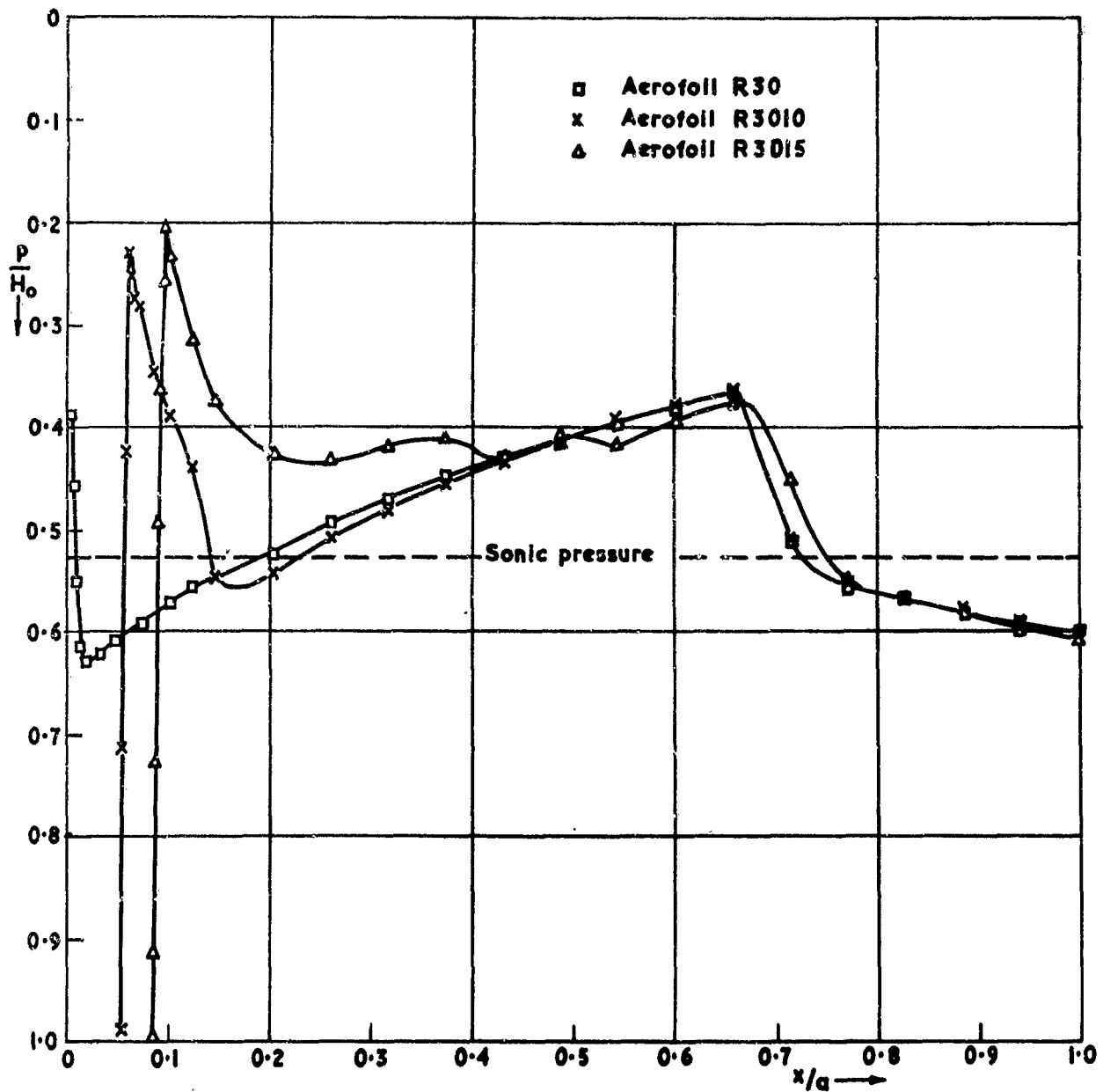


Comparison of upper-surface pressure on the sharp and blunt leading-edged  
aerofoils at  $M_0 = 0.80$

27 838  
FIG. 9 (b)



27 838  
FIG. 10(a)

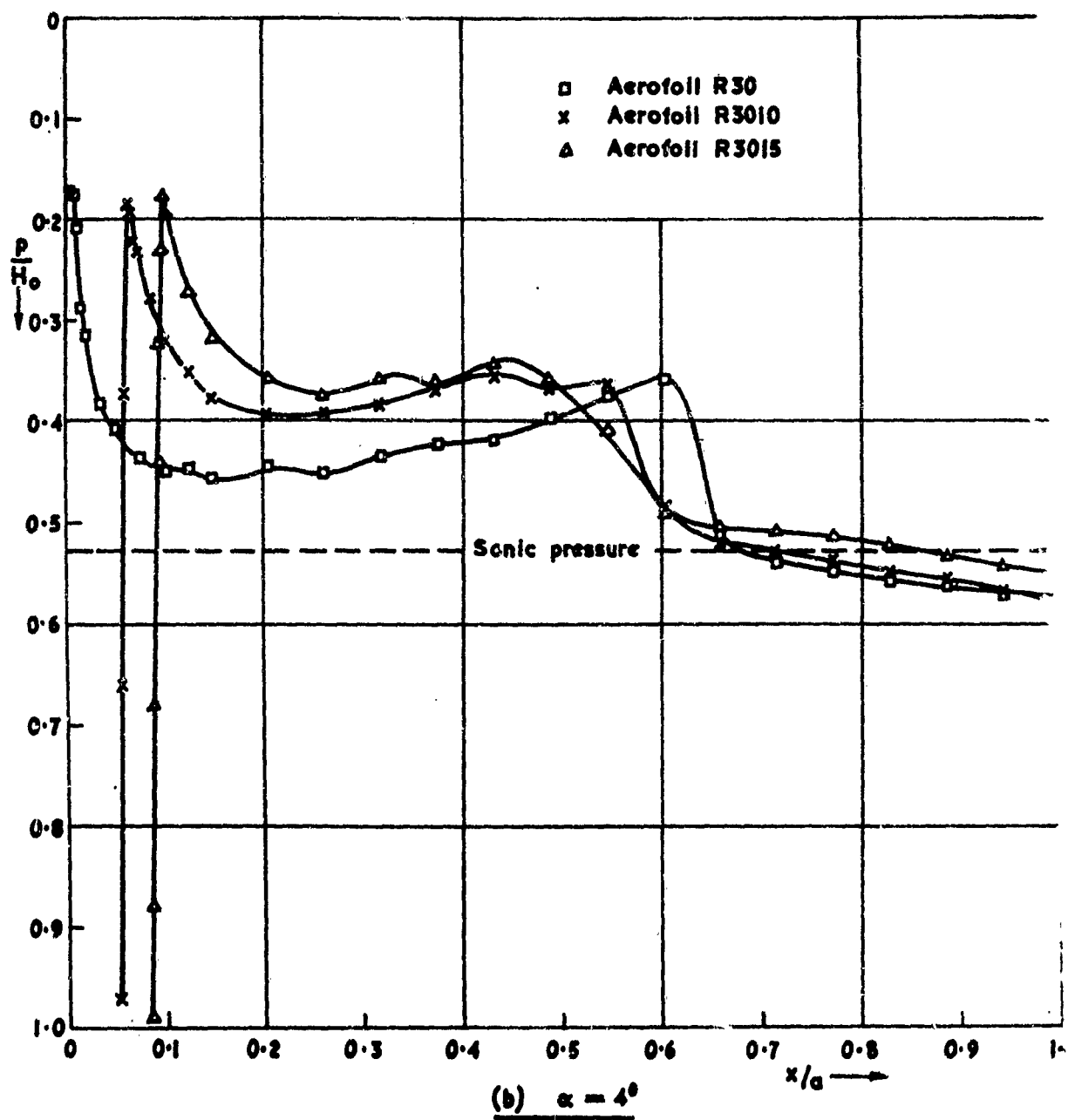


(a)  $\alpha = 2^\circ$

Comparison of upper-surface pressures on the sharp and blunt leading-edged aerofolils at

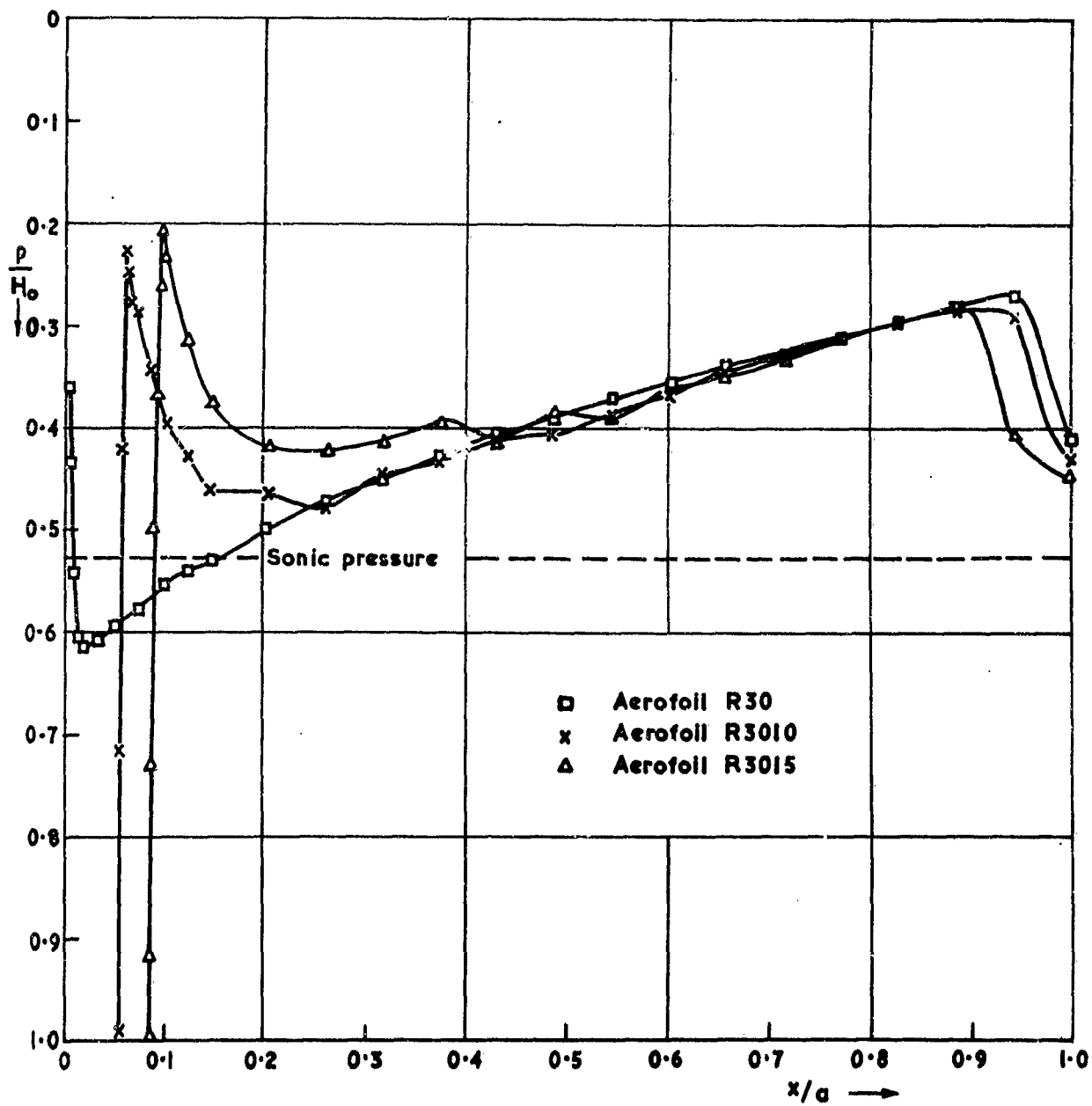
$M_0 = 0.90$

27 038  
FIG. 10(b)



27838

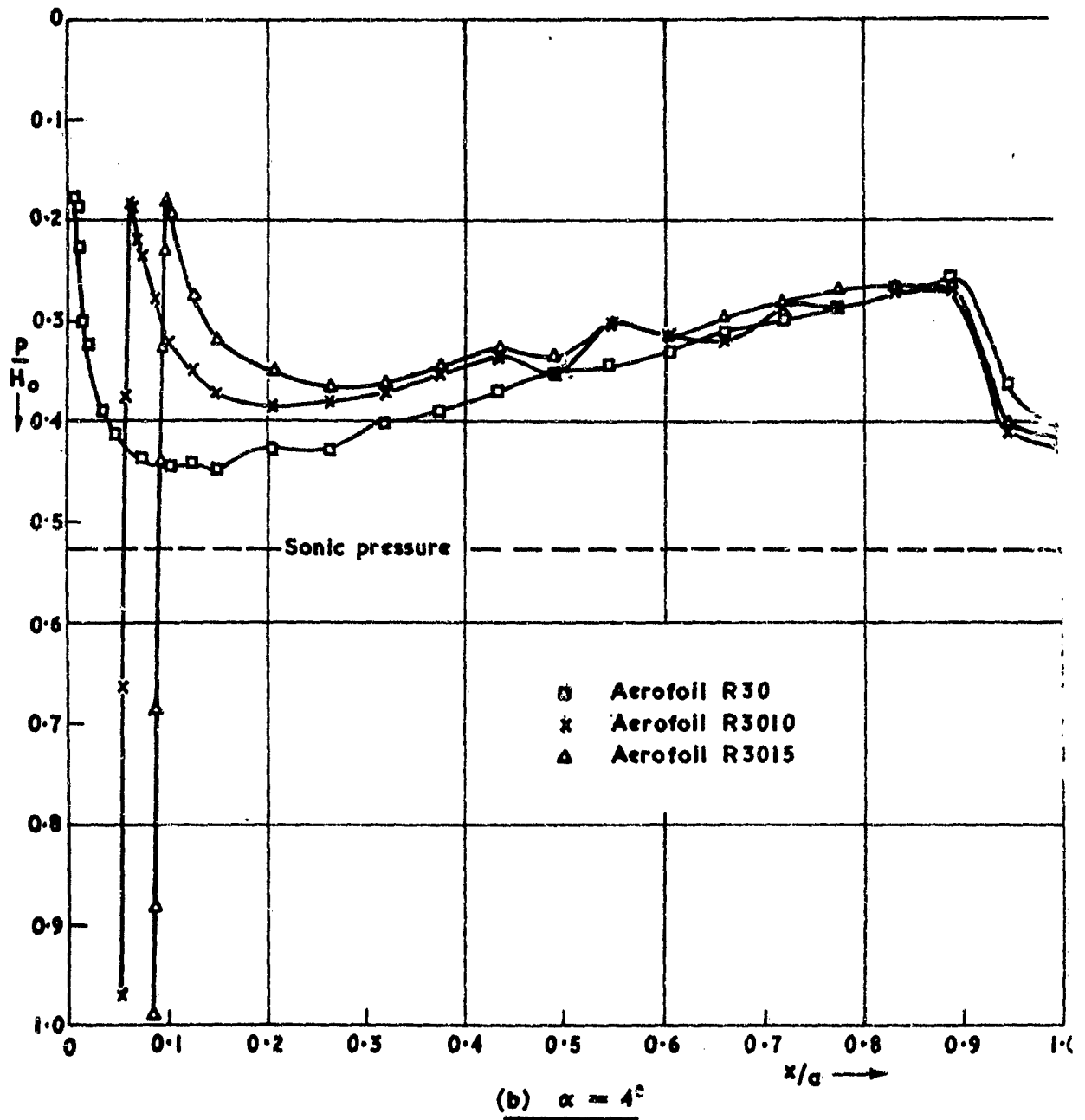
FIG. 11 (a)

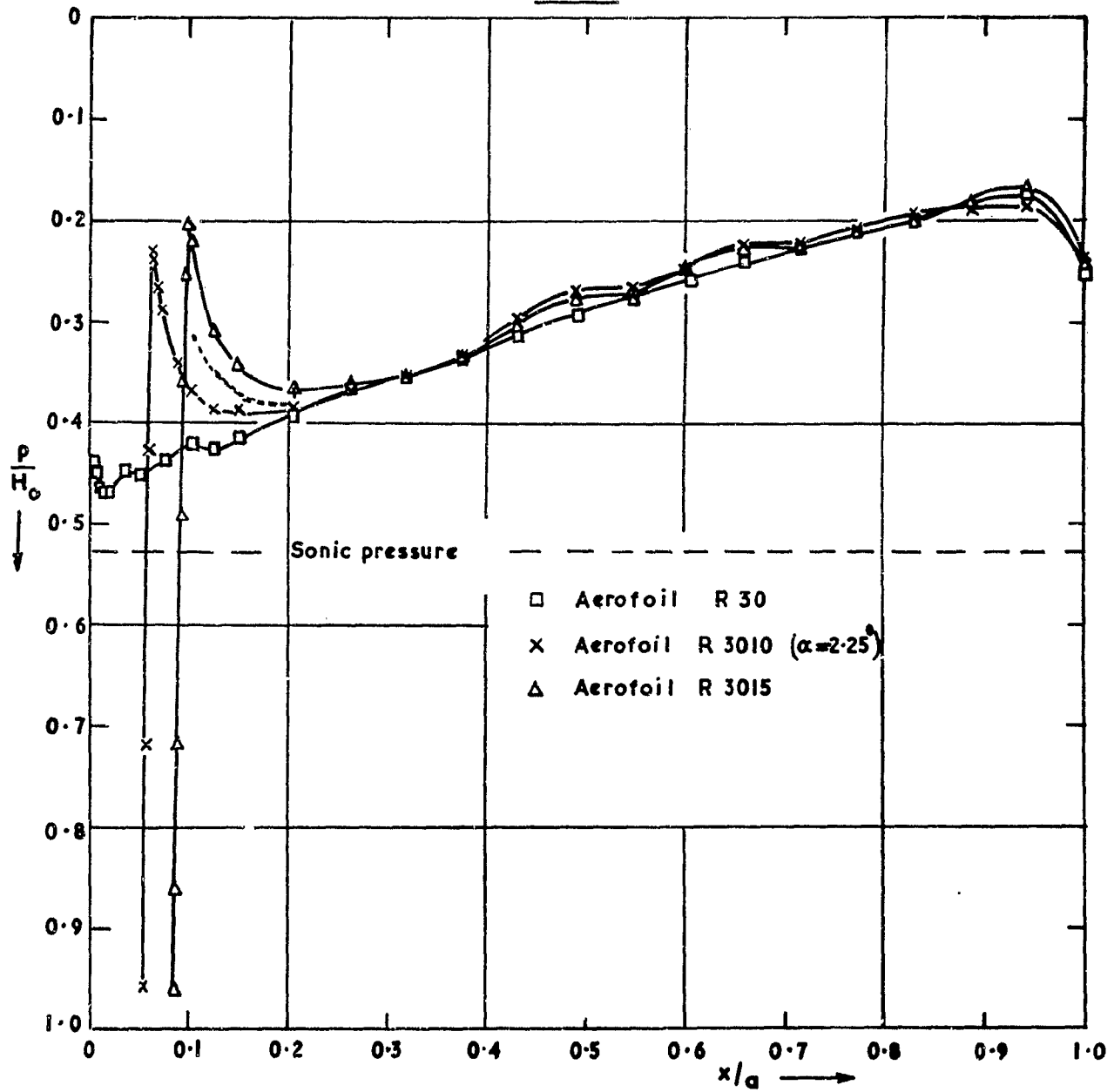


(a)  $\alpha = 2^\circ$

Comparison of upper-surface pressures on the sharp and blunt leading-edged aerofolils  
at  $M_0 = 1.00$

27 838  
FIG. 11 (b)

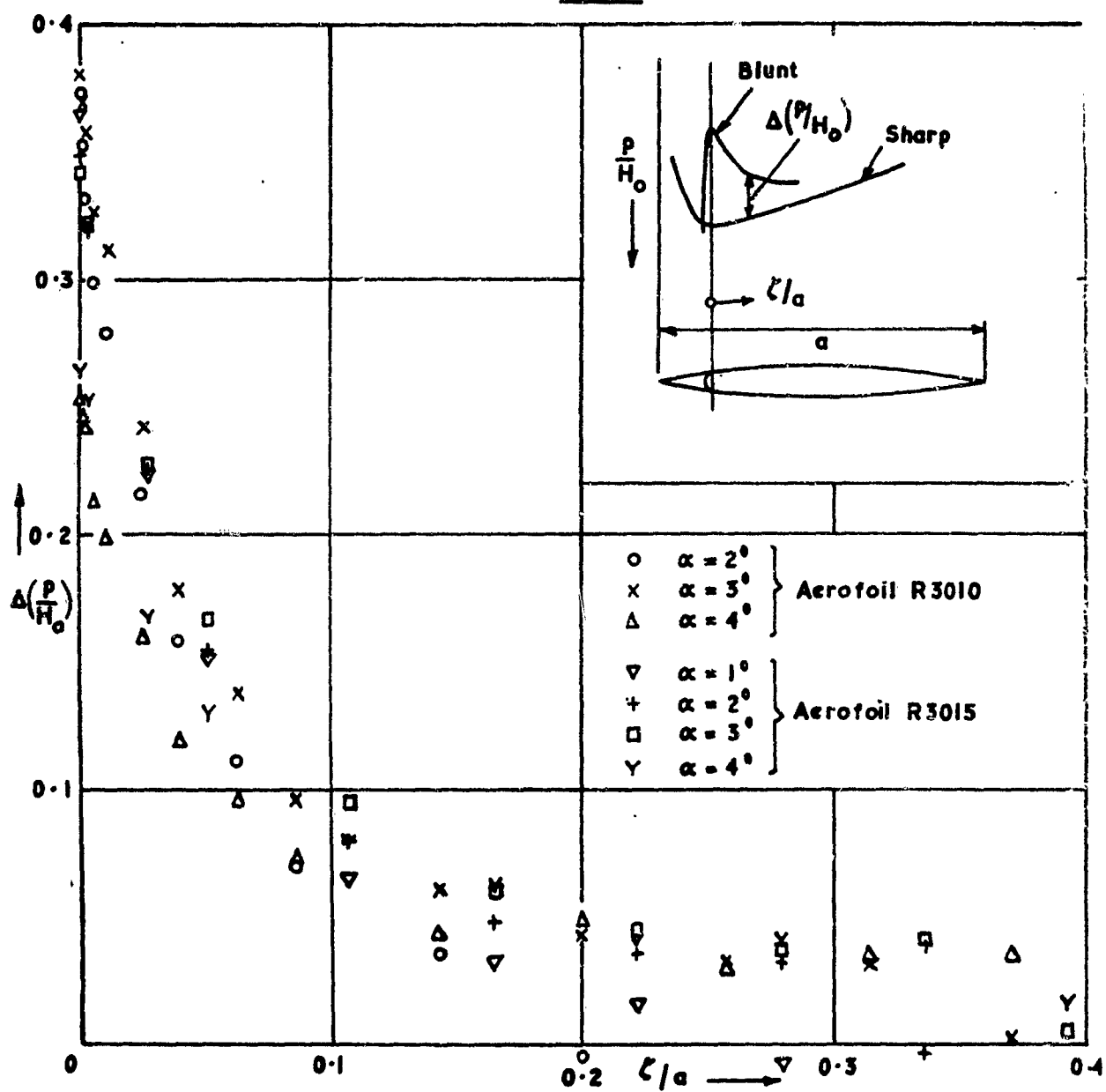




Comparison of upper-surface pressures on the sharp and blunt leading-edged  
aerofoils at  $M_0 = 1.40$

(a)  $\alpha = 2^\circ$

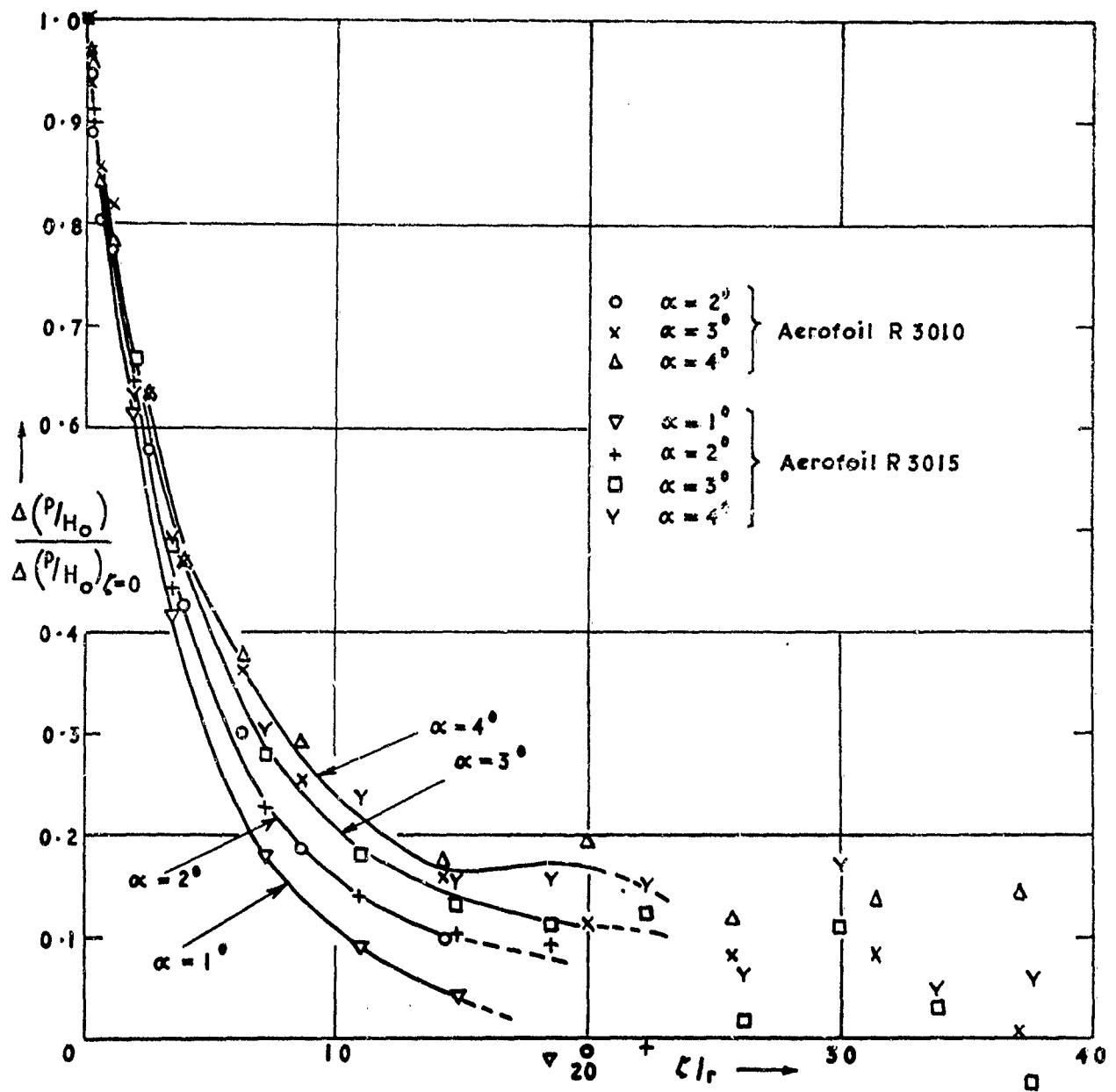
27836  
FIG. 13



Induced pressure differences due to leading-edge blunting

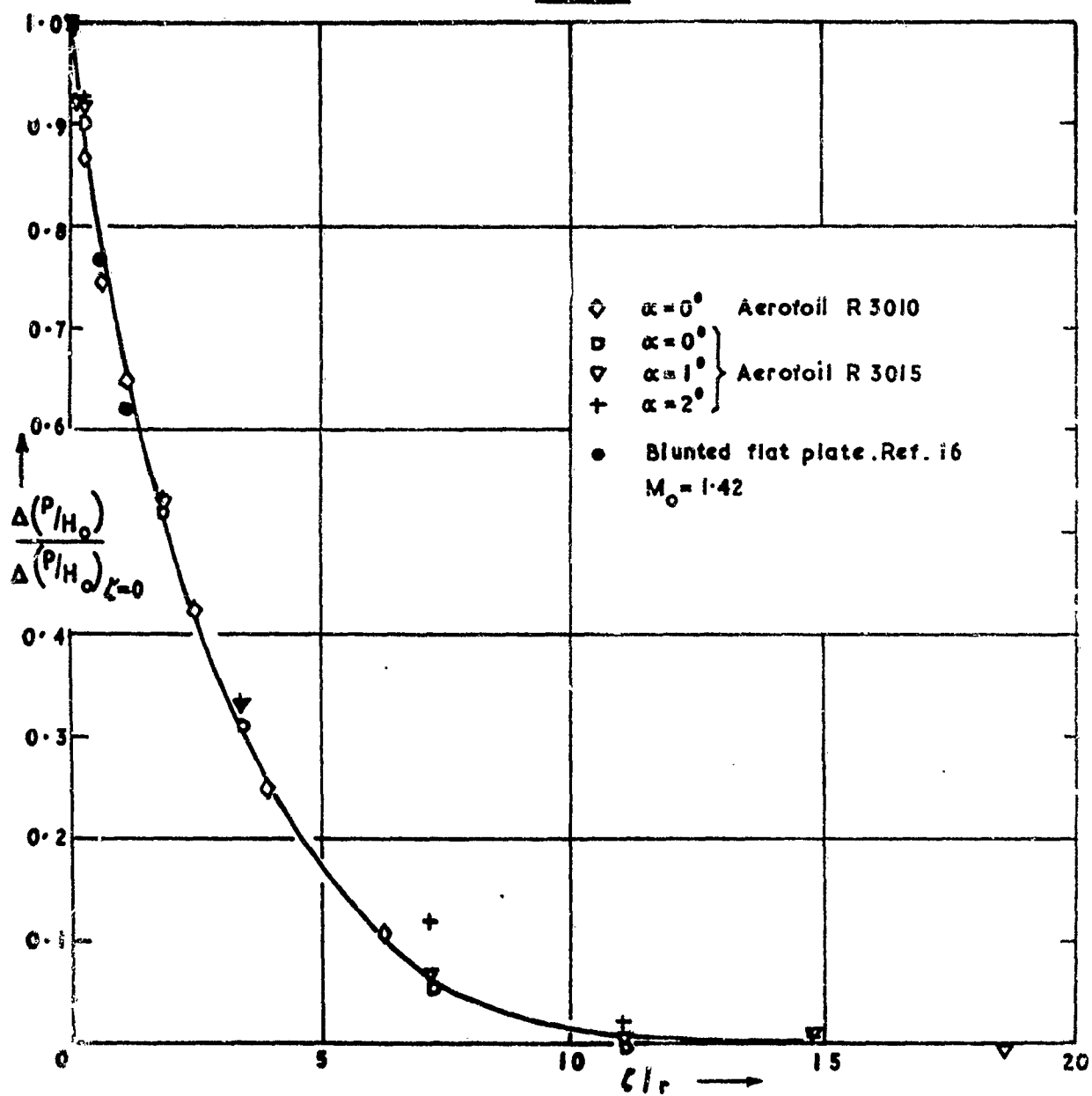
$M_0 = 1.00$

27838  
FIG. 14



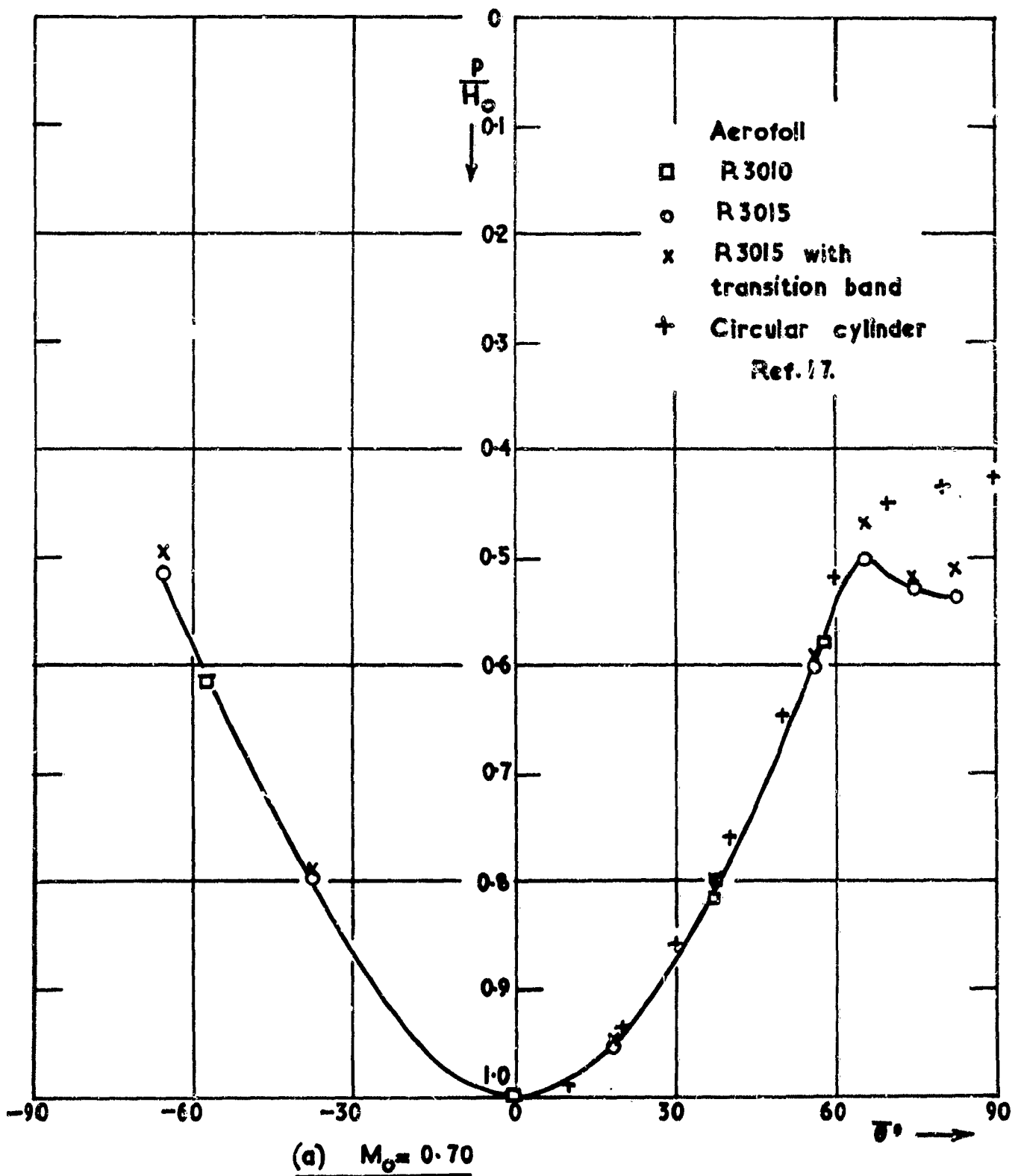
Correlation of induced pressure differences due to leading-edge blunting  
 $M_o = 1.00$

27838  
FIG. 15



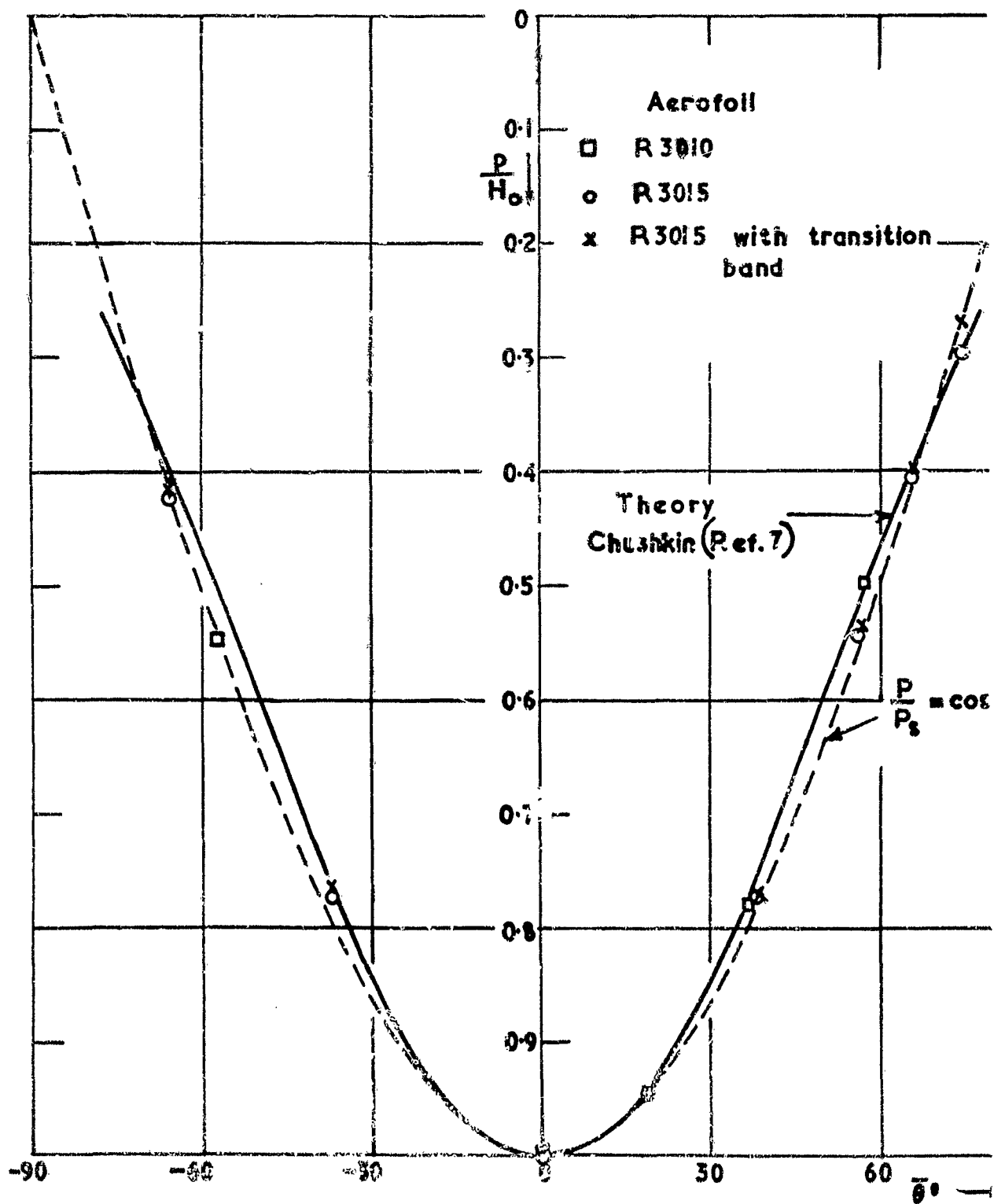
Correlation of induced pressure differences due to leading-edge blunting  
 $M_0 = 1.40$

27 838  
FIG.16(a)



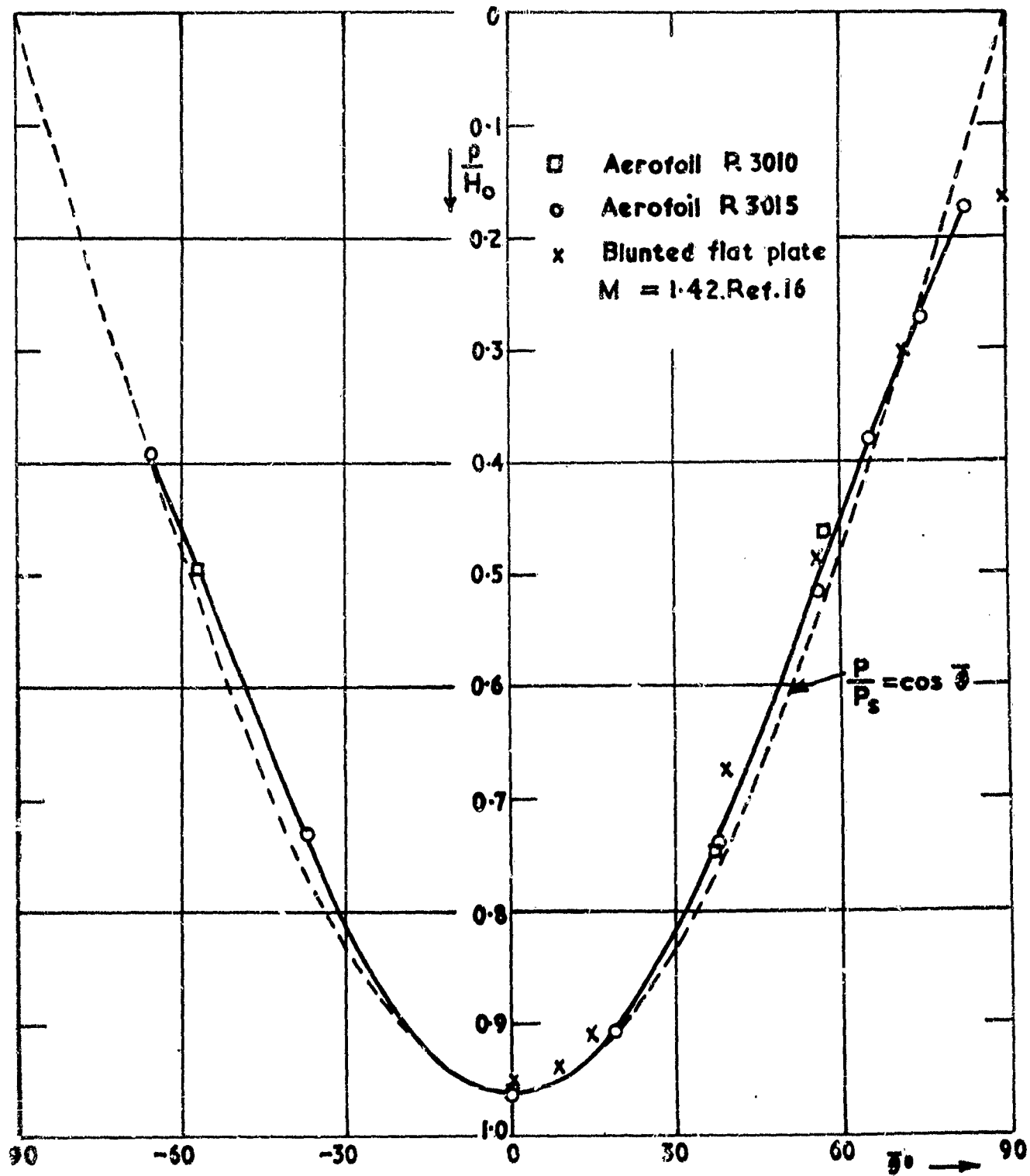
Pressures on cylindrical leading-edge of constant radius at zero incidence

27 838  
FIG. 16 (b)



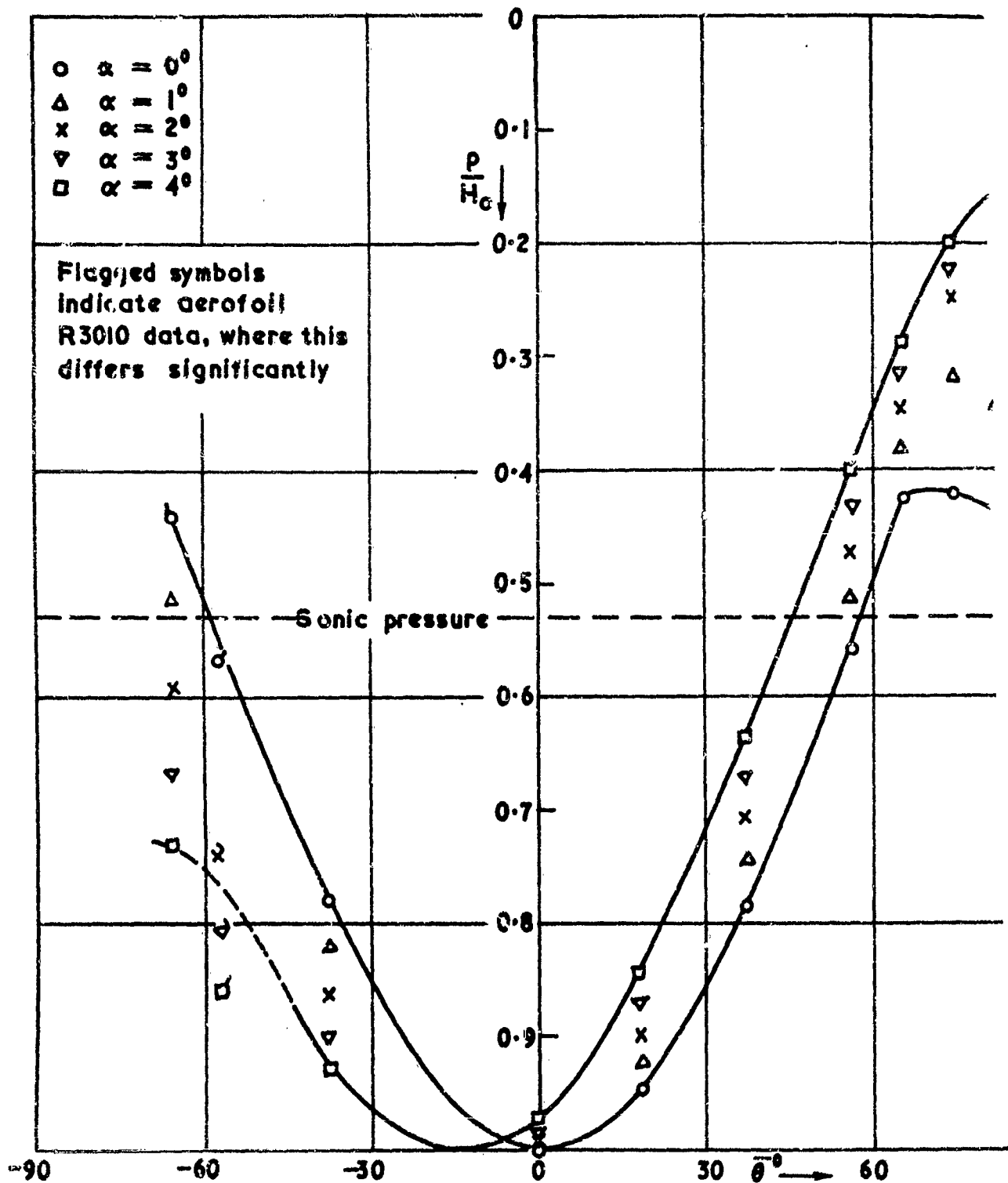
(b)  $M_0 = 1.00$

27 838  
FIG.16(c)

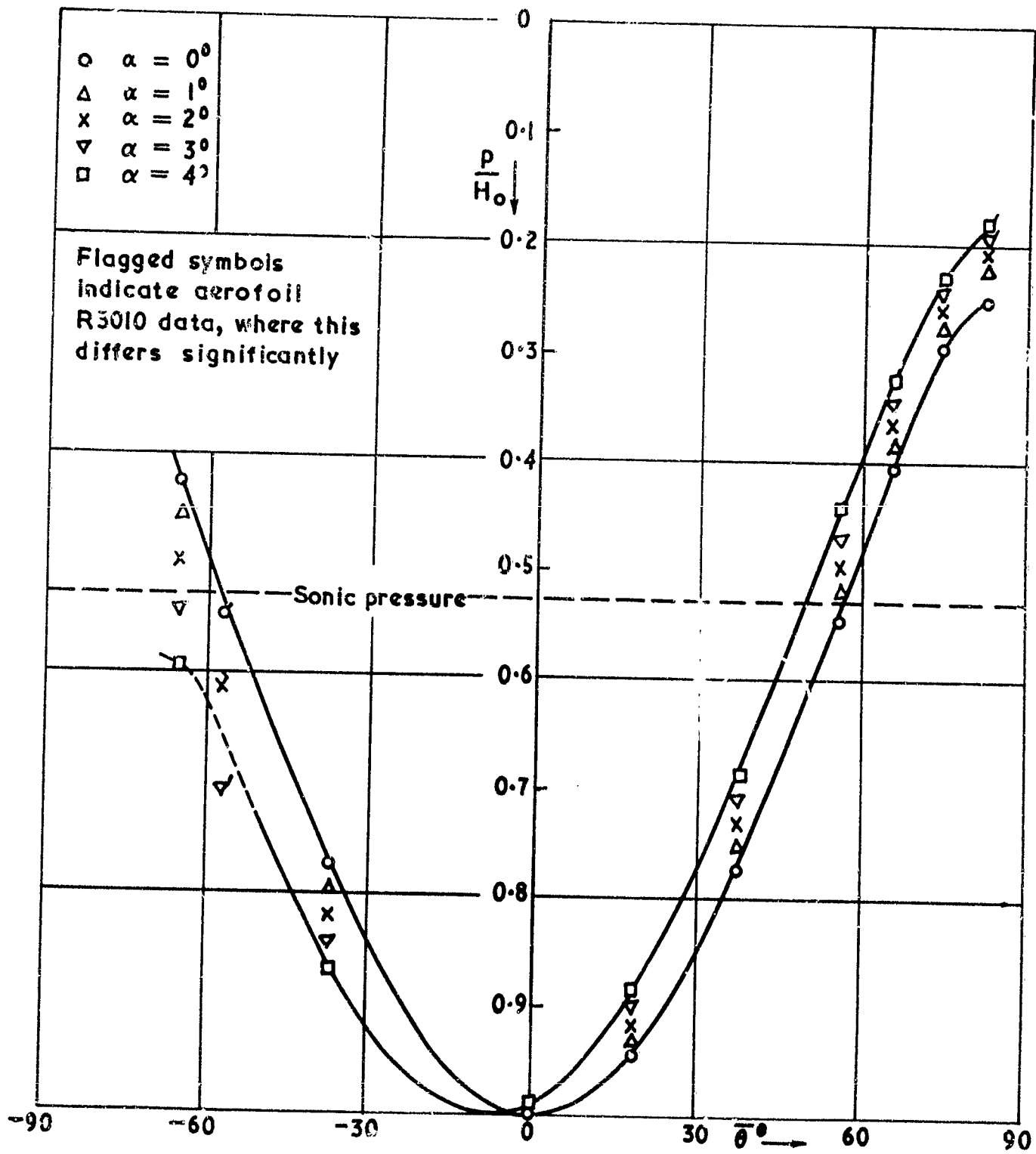


(c)  $M_\infty = 1.40$

27 836  
FIG. 17(a)

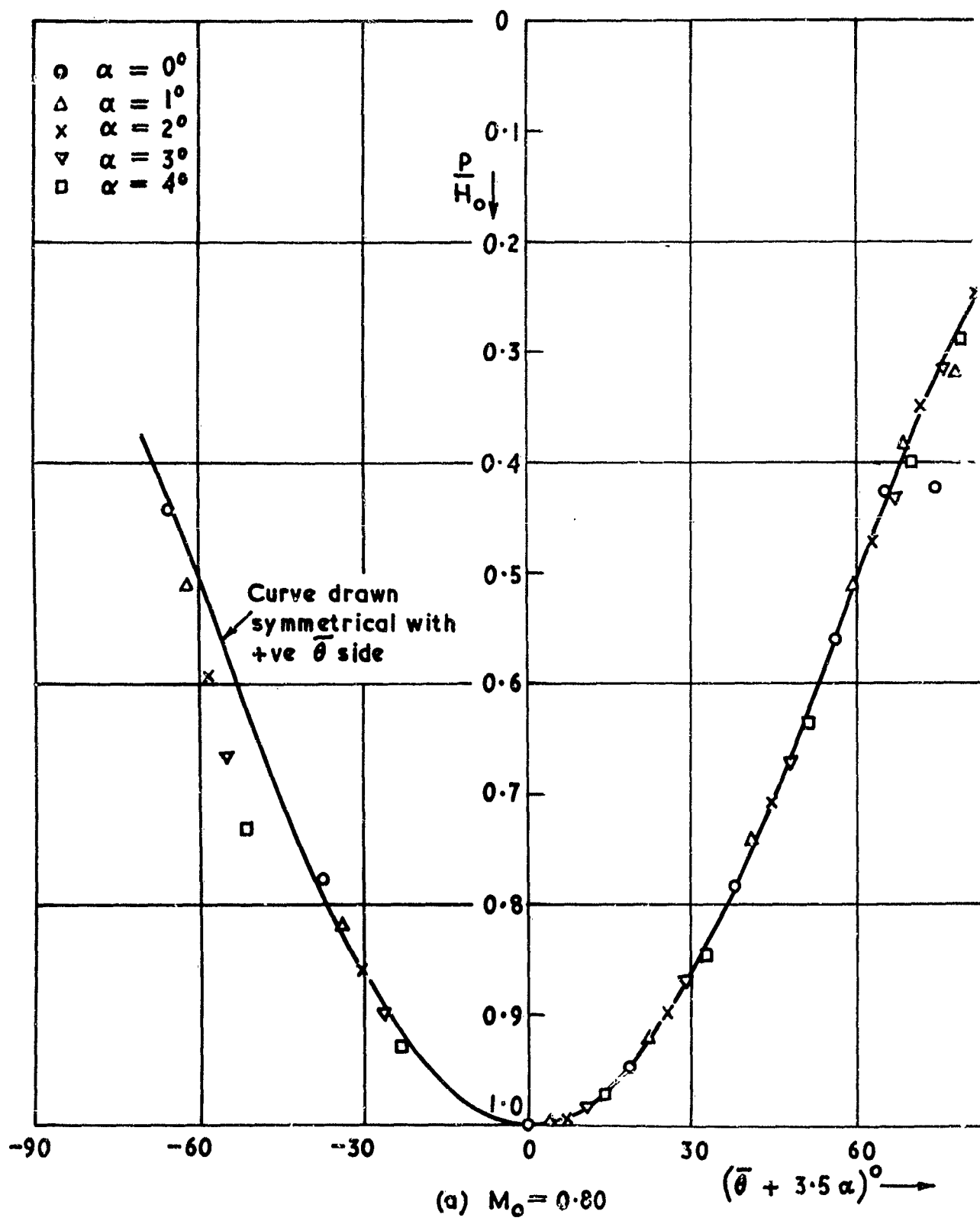


27838  
FIG. 17(b)



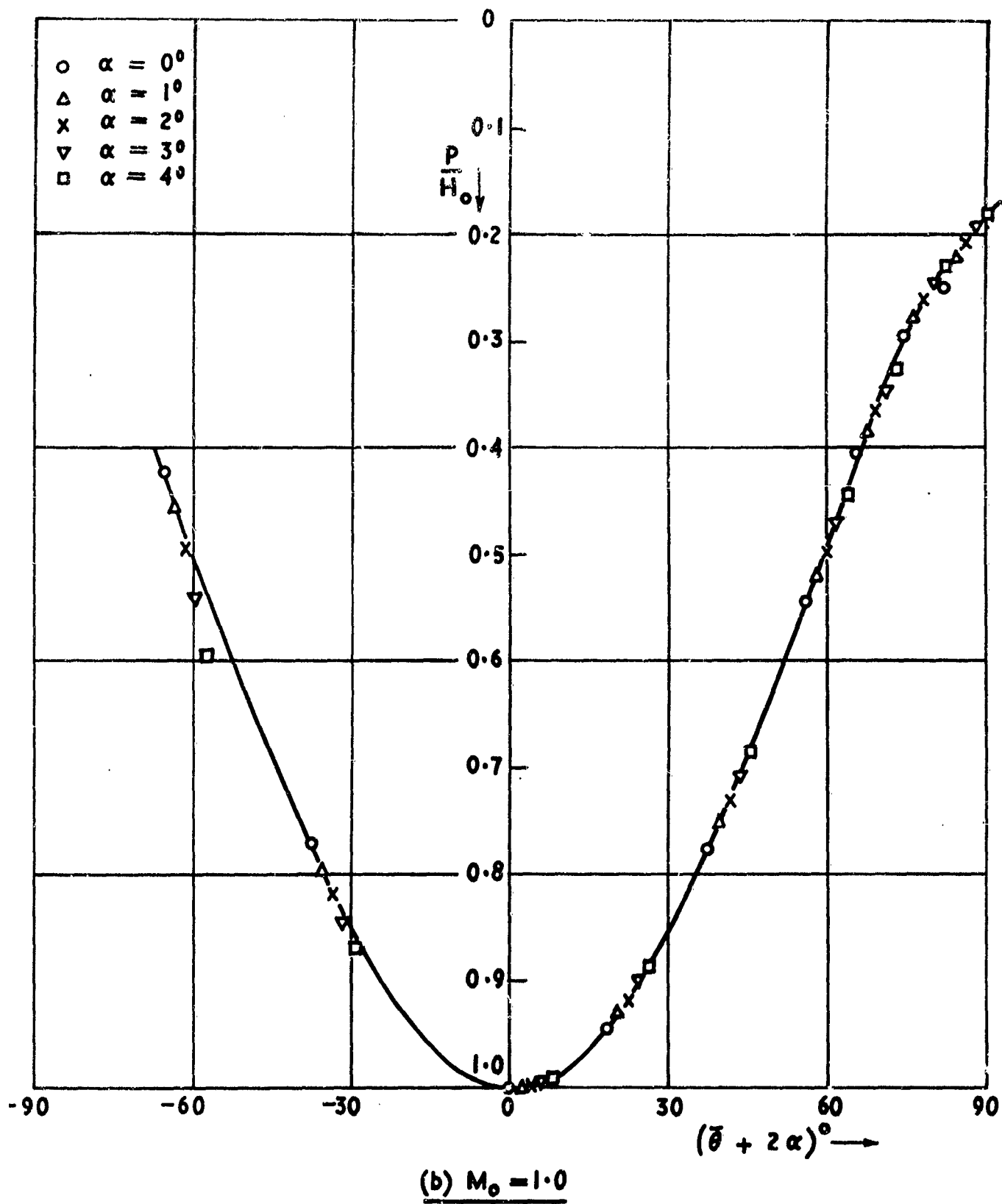
(b)  $M_o = 1.0$

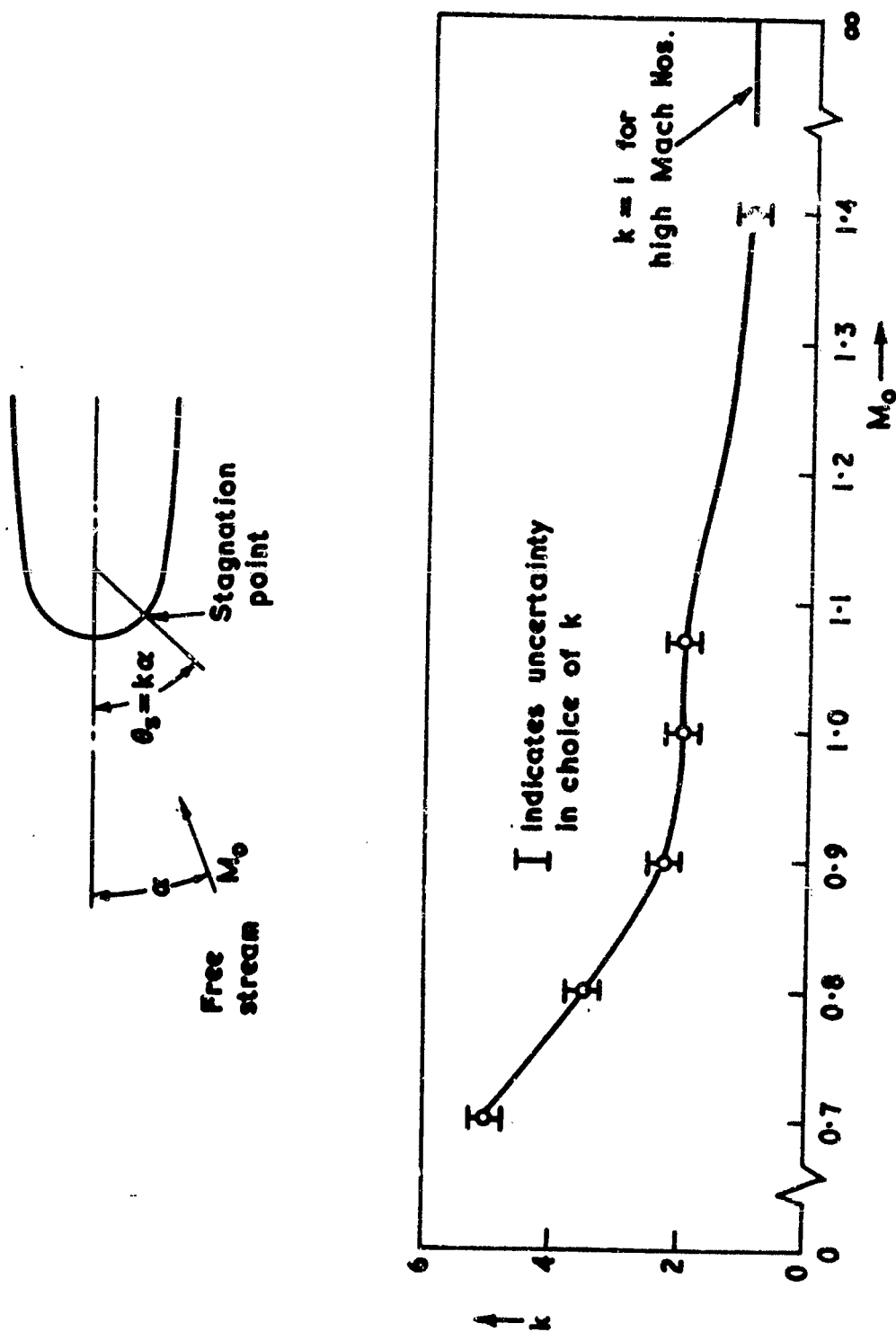
27838  
FIG 18 (a)



Correlation of pressure distributions at incidence on leading-edge of  
airfoil R 3015

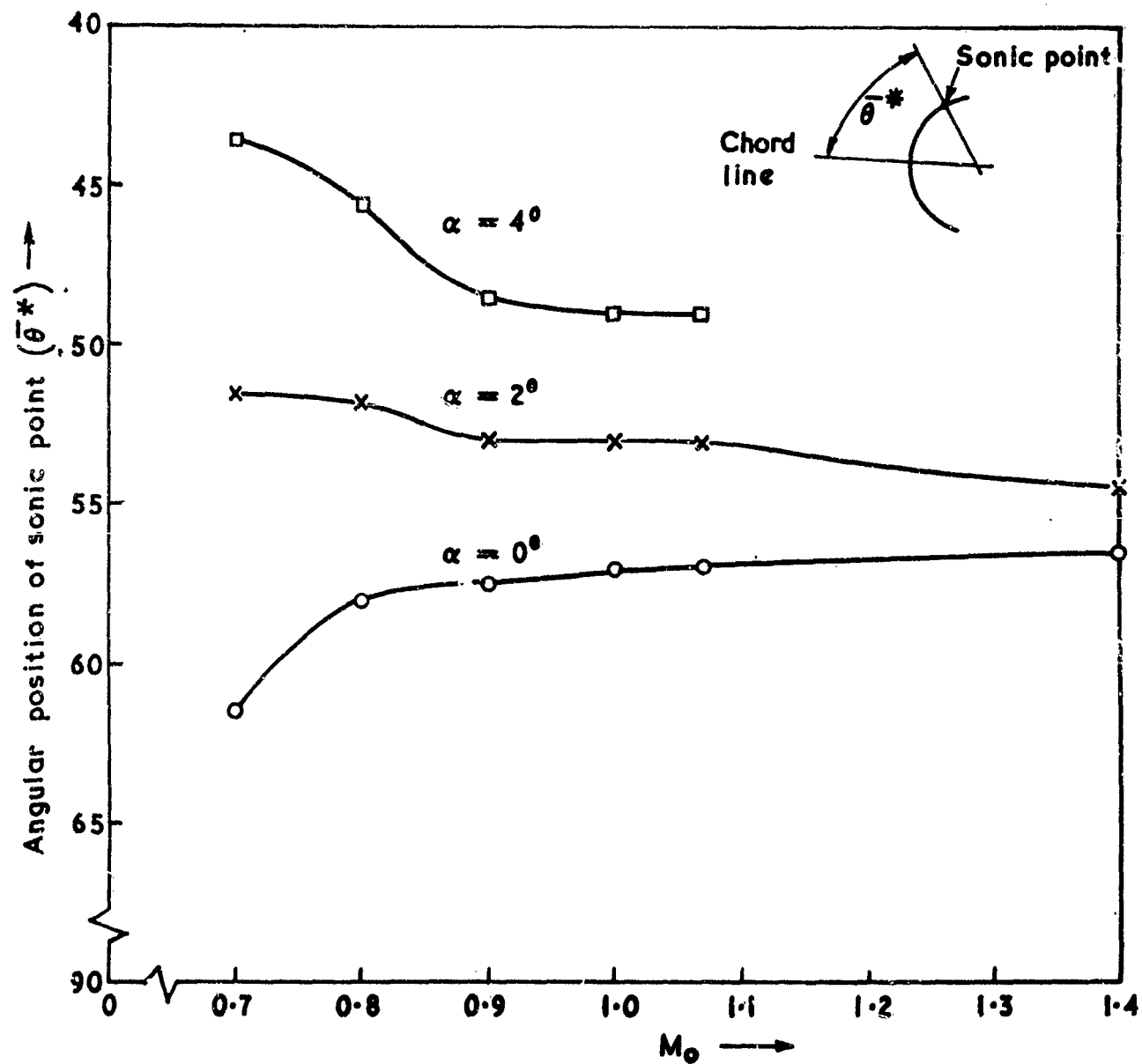
27838  
FIG. 18 (b)





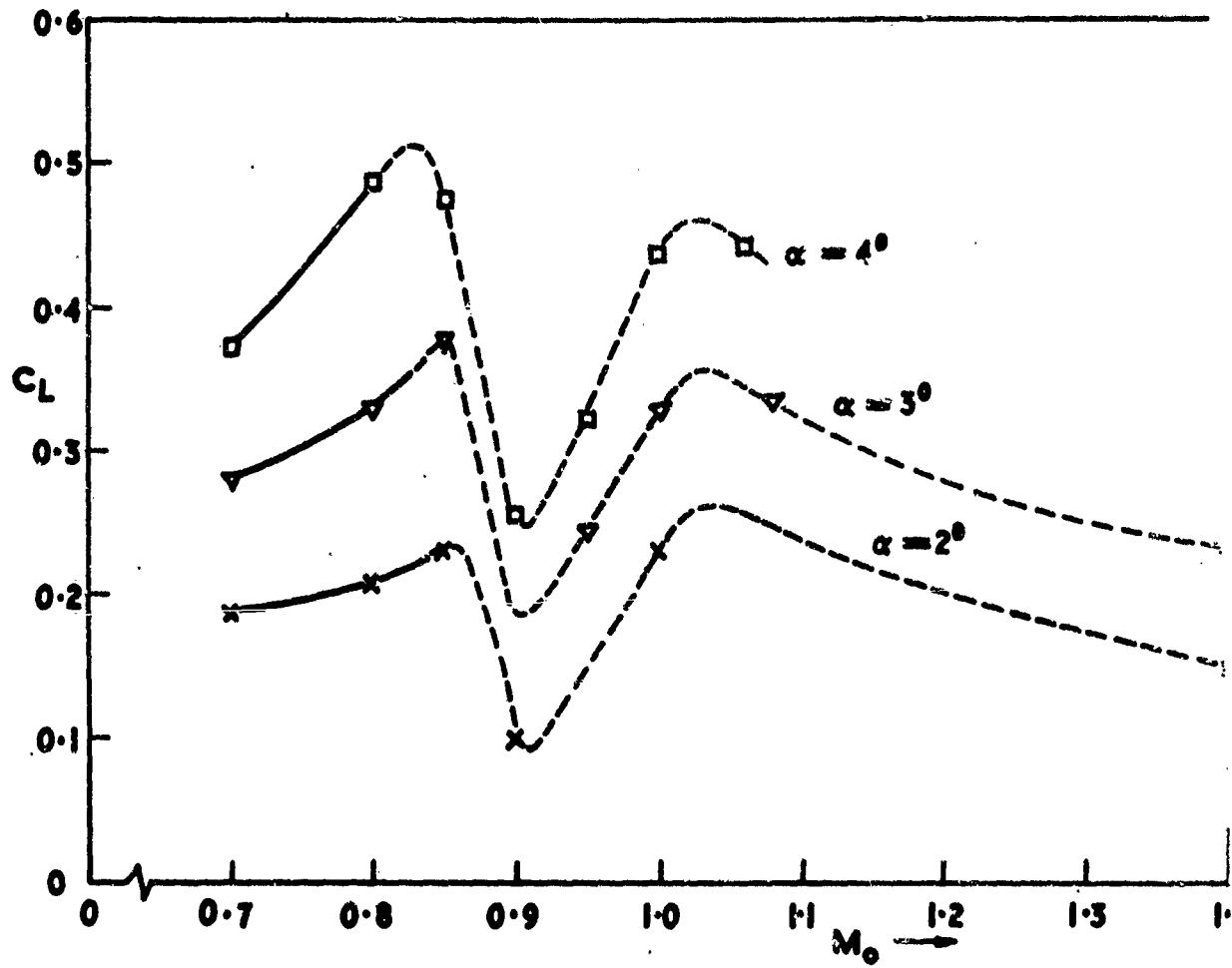
Rate of angular movement ( $k$ ) of stagnation point on aerofolls R 3015 and

R3010 with incidence. Effect of Mach number



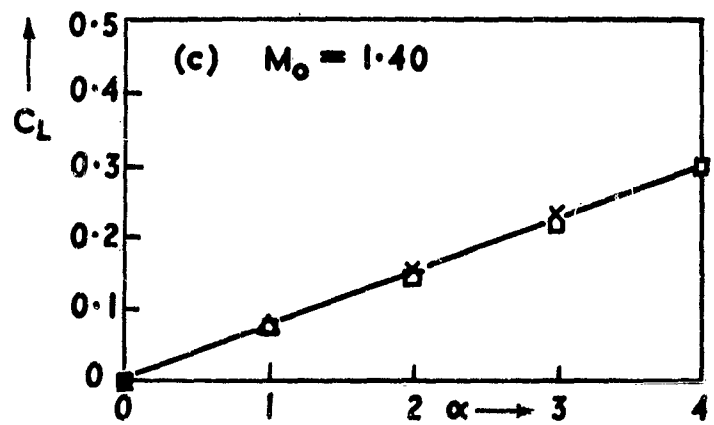
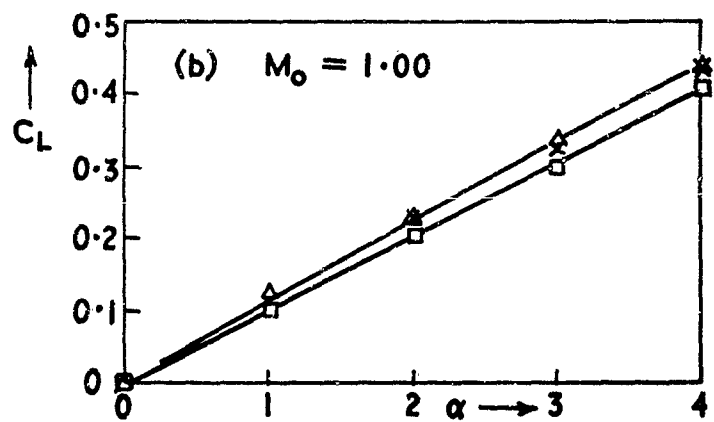
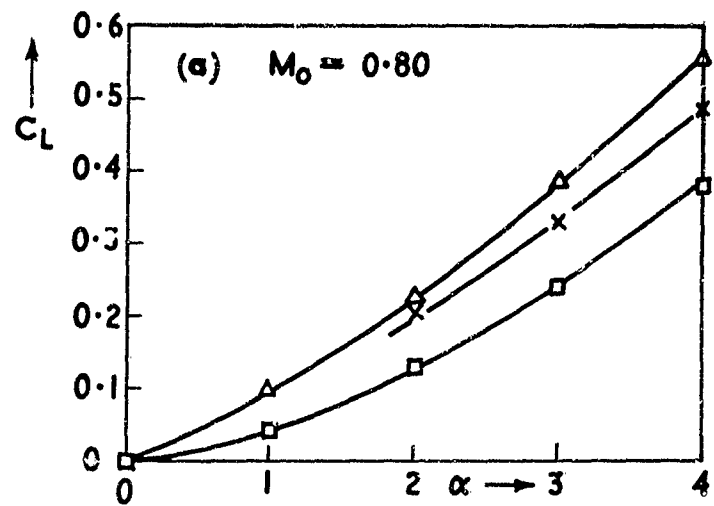
Movement of sonic point on aerofolis R3010 and R3015 with  
Mach number for various incidences

27 838  
FIG. 21



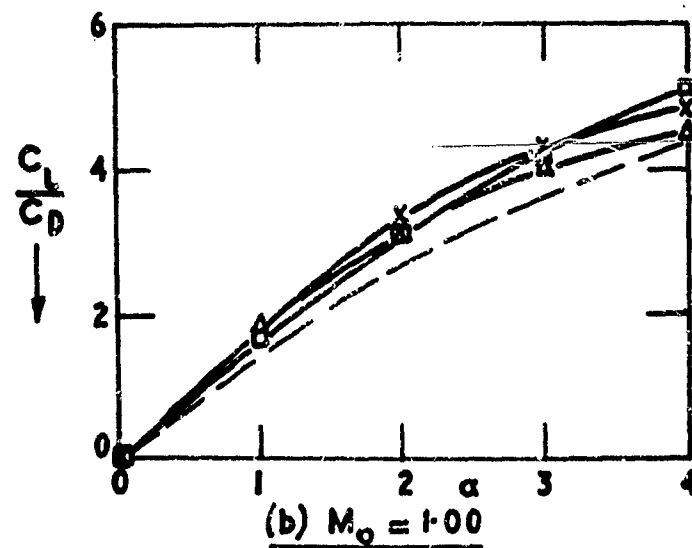
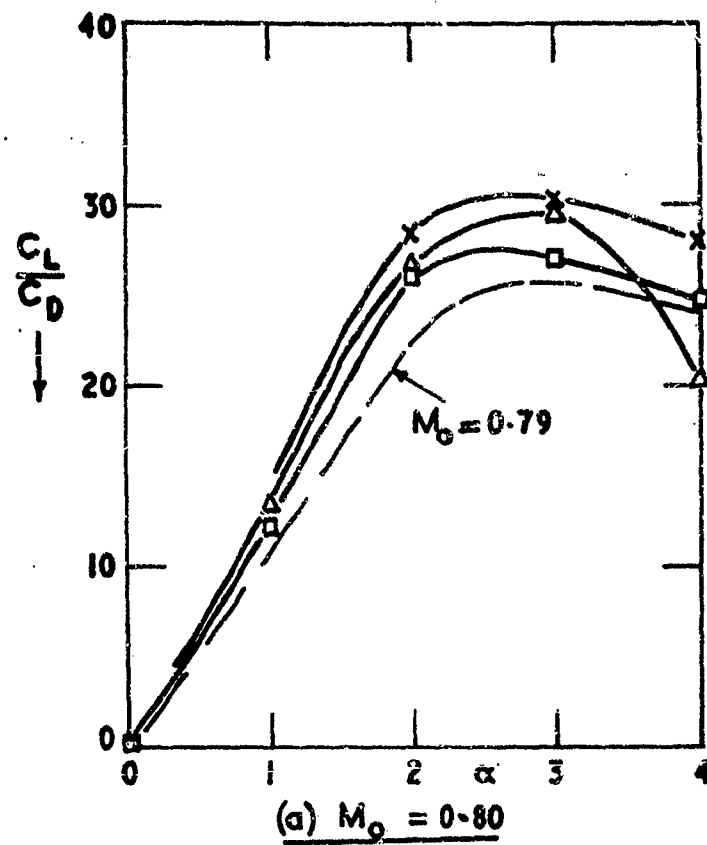
Variation of lift coefficient on R3010 with Mach number for various  
incidences

27 838  
FIG. 22 (a-c)



$\square$  Aerofoil R 30  
 $\times$  Aerofoil R 3010  
 $\Delta$  Aerofoil R 3015

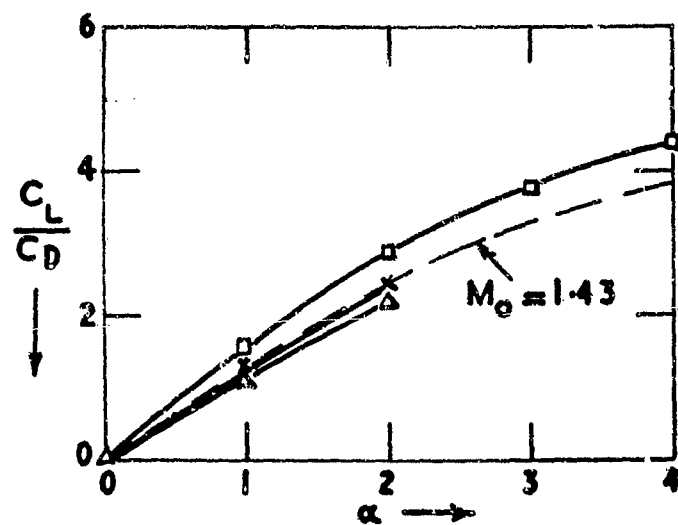
Comparison of lift coefficients for sharp and blunt  
leading-edged aerofoils. Variation with incidence.



Aerofoil  
 □ R30  $\tau = 0.084$   
 x R3010  $\tau = 0.088$   
 Δ R3015  $\tau = 0.092$   
 --- Sharp L.E.  $\tau = 0.092$

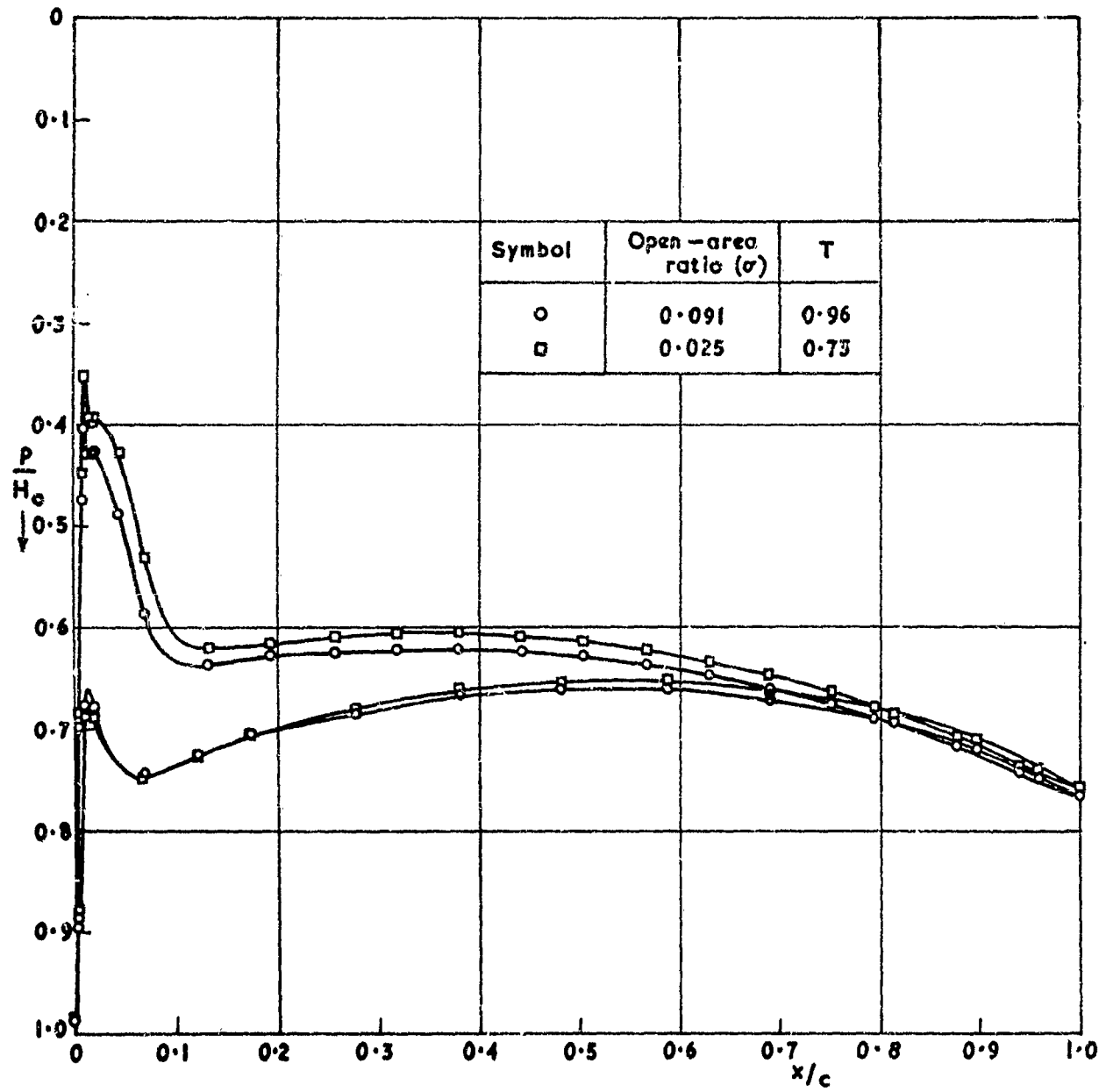
Comparison of lift-drag ratios for sharp and blunt leading-edged aerofoils. Variation with incidence.

27 838  
FIG. 23 (c)



(c)  $M_0 \approx 1.40$

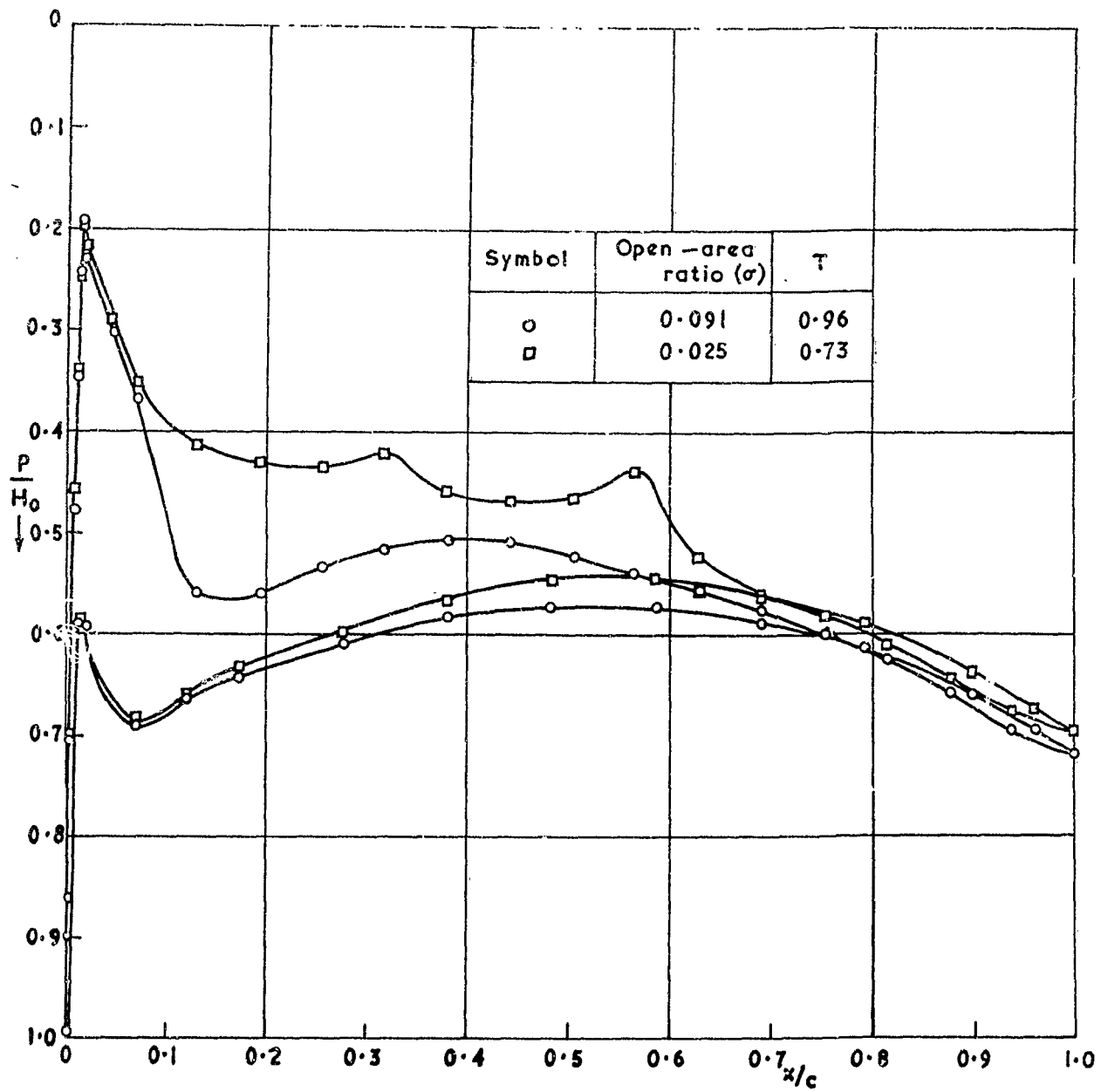
27 838  
FIG. 24(a)



(a)  $M_0 = 0.70$ ,  $\alpha = 2^\circ$

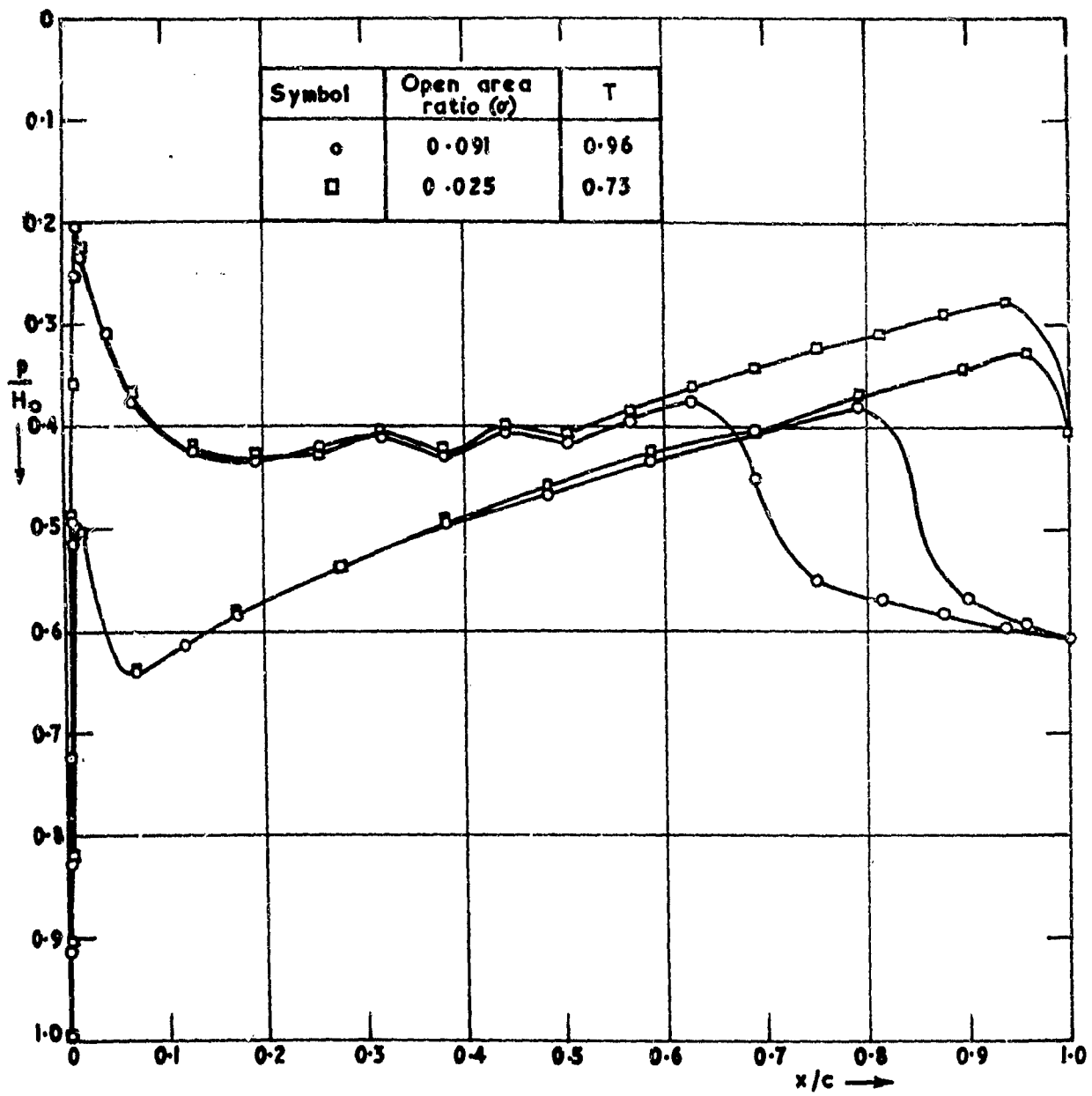
Effect on pressure distribution of varying wall slot opening.      Aerotoll R 3015

27 838  
FIG. 24 (b)



(b)  $M_0 = 0.80$ ,  $\alpha = 2^\circ$

27 838  
FIG. 24 (c)



(c)  $M_0 = 0.90, \alpha = 2^\circ$